Distributed Adaptive Fixed-Time Fault-Tolerant Control for Multiple 6-DOF UAVs With Full-State Constraints Guarantee

Zhang, Boyang; Sun, Xiuxia; Lv, Maolong; Liu, Shuguang; Li, Le

DOI
10.1109/JSYST.2021.3128973

Publication date
2022

Document Version
Final published version

Published in
IEEE Systems Journal

Distributed Adaptive Fixed-Time Fault-Tolerant Control for Multiple 6-DOF UAVs With Full-State Constraints Guarantee

Boyang Zhang, Xiuxia Sun, Maolong Lv, Shuguang Liu, and Le Li

***Abstract*—In contrast with most existing results concerning unmanned aerial vehicles (UAVs) wherein material points or only attitude/longitudinal dynamics are considered, this article proposes a distributed fixed-time fault-tolerant control methodology for networked fixed-wing UAVs whose dynamics are six-degree-of-freedom with twelf-state-variables subject to actuator faults and full-state constraints. More precisely, state transformations with the scaling function are devised to keep the involved velocity and attitude within their corresponding constraints. The fixed-time property is obtained in the sense of guaranteeing that the settling time is lower bounded by a positive constant, which is independent of initial states. The actuator faults as well as the network induced errors are handled via the bound estimation approach and well-defined smooth functions. By strict Lyapunov arguments, all closed-loop signals are proved to be semiglobally uniformly ultimately bounded, and the tracking errors of velocity and attitude converge to the residual sets around origin within a fixed time.**

***Index Terms*—Fault-tolerant control (FTC), fixed-time convergence, full-state constraints, six-degree-of-freedom (DOF) fixed-wing unmanned aerial vehicles (UAVs).**

NOMENCLATURE

ϕ_i	Roll angle.
ϕ_r	Reference command of ϕ_i.
ψ_i	Yaw angle.
ψ_r	Reference command of ψ_i.
ρ	Air density.
θ_i	Pitch angle.
θ_r	Reference command of θ_i.
m_i	Vehicle mass.
p_i	Angular velocity in *X* of body fixed frame.
q_i	Angular velocity in *Y* of body fixed frame.
r_i	Angular velocity in *Z* of body fixed frame.
u_i	Linear velocity in *X* of body fixed frame.
V_i	Total speed in body fixed frame.
v_i	Linear velocity in *Y* of body fixed frame.
V_r	Reference command of V_i.
w_i	Linear velocity in *Z* of body fixed frame.
α_i	Attack angle.
$\bar{c}_i$	Mean aerodynamic chord.
$\bar{q}_i$	Dynamic pressure.
β_i	Sideslip angle.
$\boldsymbol{\delta}_i$	Flight control surface.
$\boldsymbol{S}(\bullet)$	Skew-symmetric matrix.
δ_{ai}	Aileron angular deflection.
δ_{ei}	Elevator angular deflection.
δ_{ri}	Rudder angular deflection.
$\lambda_{\max}(\bullet)$	Maximum eigenvalue of a matrix.
$\lambda_{\min}(\bullet)$	Minimum eigenvalue of a matrix.
$\Re^m$	Real m-vector.
$\Re^{m\times n}$	Real $m \times n$ matric.
$\mathrm{SO}(3)$	Third-order special orthogonal group.
b_i	Wingspan.
S_i	Wing surface area.
$\boldsymbol{\omega}_i$	Noninertial expression of angular velocity.
$\boldsymbol{\varphi}_i$	Attitude described by Euler angles.
$\boldsymbol{\varphi}_r$	Reference command of $\boldsymbol{\varphi}_i$.
$\boldsymbol{d}_{\omega i}$	External disturbances in angular velocity.
$\boldsymbol{d}_{vi}$	External disturbances in velocity.
$\boldsymbol{F}_i$	Aerodynamics force.
$\boldsymbol{g}$	Gravity acceleration.
$\boldsymbol{J}_i$	Inertia tensor.
$\boldsymbol{N}_i$	Aerodynamics moment.
$\boldsymbol{p}_i$	Inertial position.
$\boldsymbol{T}_i$	Thrust vector along x body axis.
$\boldsymbol{v}_i$	Noninertial expression of the linear velocity.

Manuscript received 22 March 2021; revised 18 August 2021 and 29 October 2021; accepted 7 November 2021. Date of publication 8 December 2021; date of current version 26 August 2022. This work was supported by the Aeronautical Science Foundation of China under Grant 20155896025. *(Corresponding author: Maolong Lv.)*

Boyang Zhang, Xiuxia Sun, and Shuguang Liu are with the Department of Equipment Management and Unmanned Aerial Vehicle Engineering, Air Force Engineering University, Xi'an 710051, China (e-mail: boyang_530@163.com; gcxysxx@126.com; dawny_liu@163.com).

Maolong Lv is with the College of Air Traffic Control and Navigation, Air Force Engineering University, Xi'an 710051, China, and also with the Delft Center for Systems and Control, Delft University of Technology, 2628 CD Delft, The Netherlands (e-mail: m.lyu@tudelft.nl).

Le Li is with the School of Marine Science and Technology, Northwestern Polytechnical University, Xi'an 710051, China (e-mail: leli@nwpu.edu.cn).

Digital Object Identifier 10.1109/JSYST.2021.3128973

I. INTRODUCTION

COORDINATED flight of multiple fixed-wing unmanned aerial vehicles (UAVs) has been extensively studied over the past decades, due to its important role in achieving flexibility and cost effectiveness of mission cooperation [1], [2]. In general, coordinated control problem has been investigated in several aspects, including formulating and maintaining a particular formation shape for UAVs in a group [3], and synchronous tracking of velocity and attitude for UAV formation [4]. Fixed-wing UAVs are peculiar in terms of six-degree-of-freedom (DOF) dynamics, and these peculiarities should be borne in mind when formulating a control law.

A. Related Research

As technologies advance, the distributed control strategy has been attached tremendous attentions and is desirable for UAV groups due to the fact that the global information is no longer required in control design, while providing the scalability and tackling the vulnerability of centralized UAVs tasked to control a group [5], [6]. Driven by the emerging distributed cooperative control research on multiple UAVs, some results have appeared in [7]–[12]. To list a few, Yu *et al.* [7] presented a distributed cooperative control design for networked UAVs against actuator faults and model uncertainties. In [8], for longitudinal synchronization tracking of multiple UAVs, a distributed cooperative fault-tolerant controller was proposed in the presence of input saturation. Based on the swarm intelligence, Wang *et al.* [9] proposed a distributed model predictive approach for coordination control of multiple UAVs. In [10], with path-following vector fields, the UAV group achieves a circular motion around the target. Notably, most existing papers on the problem analyze UAV dynamics models as material points [9]–[12], and focus on the attitude or longitudinal dynamics [7], [8], which is an excessive and unnecessary simplification in practice. Therefore, the motivation of investigation on six-DOF UAV dynamics naturally arises.

In ideal conditions, the aforementioned control methods can achieve good control results with asymptotic convergence. However, in real flight conditions, there is strict requirement for convergence time, which mainly influences the system performances. The advanced algorithm to improve the efficiency of tracking convergence is finite-time control design. This technique has been successfully applied to UAV flights in [13]–[15]. But the main disadvantages of finite-time controls are as follows:

1) the convergence time strongly relies on the initial states;
2) considering the settling time increases with the initial states, the finite-time controls will be infeasible with large initial states.

In [16], the fixed-time control is first developed to achieve the finite-time convergence independent of initial condition. This feature successfully promotes the fixed-time stability for spacecrafts [17], surface vessels [18], surface vehicles [19], and robot manipulators [20]. However, the crucial question of designing the fixed-time control scheme for multiple UAVs still remains open.

In practical cases, state constraints are commonly found in the UAV system in the form of physical stoppage performance. The constraint consideration has been significantly important for UAVs because it ensures the avoidance of collision hazards and stability simultaneously. Some significant achievements on constrained control problem have been obtained in recent years, including model predictive control [21], use of set invariance [22], and barrier Lyapunov function [23]. Beyond these, the nonbarrier Lyapunov function was proposed to handle constraints in [24] and [25], where the constraints are guaranteed not transgressed by ensuring the boundedness of the proposed state-dependent function. Additionally, for UAVs during flight, negative factors including actuator faults, external disturbances, together with model uncertainties will degrade the control performance or even make the system unstable if being ignored. Therefore, there is an urgent need to take into account all negative factors when designing flight controllers to ensure the stability and tracking accuracy for the UAV system. Some literatures pay attention to fault-tolerant control (FTC) and disturbance rejection control for UAVs and gain some achievements in [26]–[29].

TABLE I
CONTROL MODELS AND CONTROL METHODS FOR EXISTING WORKS

Control Model	Existing Works	Control Method	Existing Works
2-DOF Model	[3,9-12,21]	Fault-tolerant Control	[4,7,8,13,15,26-29]
3-DOF Model	[14,30]	Constrained Control	[3,8-13,15,21,29,30]
Longitudinal Model	[8,15]	Adaptive Control	[4,7,8,10,12-14,28-30]
Attitude Model	[4,7,13,26,29]	Finite-time Control	[13-15,29]
6-DOF Model	[27,28,31,32]	Fixed-time Control	[16-20]

B. Main Contribution

Lots of works dealing with the control of the fixed-wing UAV in terms of the linearized model or separate attitude and longitudinal dynamics [7]–[12]. On the one hand, this linearized model cannot accurately reflect the motion of an UAV and the antidisturbance and fault-tolerant ability is limited; on the other hand, there can appear problems related to the transient tracking errors, which can further lead to the failure of flight. Besides, due to the presence of partially unknown nonlinearities in aircraft dynamics and the nonlinear behavior of actuators depending on different flight conditions, the adaptive controllers with antidisturbance and fault-tolerant ability are better choices than conventional controllers. Although extensive studies have been conducted for multiple UAVs and achieved accurate tracking performance in ideal flight, there are some difficulties that need to be addressed, which are as follows:

1) many studies in the research area of fixed-wing UAVs merely deal with the asymptotic convergence regardless of the requirement of the convergence time;
2) the time-varying state constrained problem of the multi-UAV system is rarely considered so far.

Motivated by the aforementioned existing works whose control models and control methods have been summarized in the Table I, the main contributions of this article are stated as follows:

1) Differently from asymptotic control for six-DOF dynamics [27], [28], [31], [32] and finite-time control for the three-DOF model [14], longitudinal dynamics [15], and attitude dynamics [13], [29], our scheme extends the design to the adaptive fixed-time FTC scheme for six-DOF UAVs.
2) Unlike most nonadaptive controls of UAV flight [3], [9]–[11], [21], [31], [32], an adaptive backstepping control is proposed with the help of bound estimation approach and well-defined smooth functions to effectively compensate for the actuator faults, external disturbances, and model uncertainties in the same time with the guarantee of global stability.
3) The scaling functions are designed to address the full-state constraints with respect to the system transformation obtained for translational and rotational dynamics, respectively. The fixed-time properties are obtained in such transformed unconstrained subsystems.

The rest of this article is organized as follows. In Section II, the problem statements and preliminaries are presented. Section III gives the cooperative distributed fixed-time control design and

stability analysis. Section IV shows the validation results, and finally, Section V concludes this article.

II. Problem Formulation and Preliminaries

A. Multi-UAV System Model

Considering a multi-UAV system consisting of N 6-DOF fixed-wing UAVs, an undirected graph $\mathcal{G} = (\mathcal{V}, \mathcal{E}, \mathcal{A})$ is concerned. The set of all UAVs is denoted by $\mathcal{V} = \{v_1, \ldots, v_N\}$ with the edges $\mathcal{E} = \{(i,j),\ i,j \in \mathcal{V}, \text{and } i \neq j\}$. Let $\mathcal{A} = a_{ij} \in \Re^{N\times N}$ denote the weighted adjacency matrix of $\mathcal{G}$. The Laplacian matrix is defined by $\mathcal{L} = \mathcal{D} - \mathcal{A}$, where $\mathcal{D} = \text{diag}\{d_1, \ldots, d_N\}$ with $d_i = \sum_{j=1}^{N} a_{ij}$. Given the leader–following structure, let $\mathcal{H} = \text{diag}\{h_1, \ldots, h_N\}$ denote the leader adjacency matrix of the graph $\mathcal{G}$. If the jth follower receives the information from the leader UAV, then $h_j > 0$, and otherwise $h_j = 0$. The neighbors of each UAV are denoted by $\mathcal{N}_i = \{v_j : (v_j,\ v_i) \in \mathcal{E}\}$.

Assumption 1: The topology of the considered multi-UAV system is an undirected graph with at least one node having access to the leading node.

B. Fixed-Wing UAV Dynamics Model

Using Newton–Euler convention, the full six-DOF dynamics of each UAV, is given by [31], [32]

$$\dot{\boldsymbol{p}}_i = \boldsymbol{R}_1(\boldsymbol{\varphi}_i)\,\boldsymbol{v}_i \tag{1}$$

$$\dot{\boldsymbol{v}}_i = -\boldsymbol{S}(\boldsymbol{\omega}_i)\,\boldsymbol{v}_i + \frac{\boldsymbol{T}_i}{m_i} + \boldsymbol{R}_1^{\mathrm{T}}(\boldsymbol{\varphi}_i)\,\boldsymbol{g} + \frac{\boldsymbol{F}_i}{m_i} + \boldsymbol{d}_{vi} \tag{2}$$

$$\dot{\boldsymbol{\varphi}}_i = \boldsymbol{R}_2^{-1}(\boldsymbol{\varphi}_i)\,\boldsymbol{\omega}_i \tag{3}$$

$$\boldsymbol{J}_i\dot{\boldsymbol{\omega}}_i = -\boldsymbol{\omega}_i \times \boldsymbol{J}_i\boldsymbol{\omega}_i + \boldsymbol{N}_i + \boldsymbol{C}(\boldsymbol{\delta}_i)\,\boldsymbol{\delta}_i + \boldsymbol{J}_i\boldsymbol{d}_{\omega i} \tag{4}$$

where $\boldsymbol{p}_i = [x_i, y_i, z_i]^{\mathrm{T}}$ denotes the inertial position, $\boldsymbol{v}_i = [u_i, v_i, w_i]^{\mathrm{T}}$ is the linear velocity in body fixed frame, $\boldsymbol{\varphi}_i = [\phi_i, \theta_i, \psi_i]^{\mathrm{T}}$ represents the attitude described by Euler angles, and $\boldsymbol{\omega}_i = [p_i, q_i, r_i]^{\mathrm{T}}$ is the noninertial expression of the angular velocity. Moreover, $\boldsymbol{T}_i = [T_{xi}, 0, 0]^{\mathrm{T}}$ denotes the thrust vector along x body axis, $\boldsymbol{\delta}_i = [\delta_{ai}, \delta_{ei}, \delta_{ri}]^{\mathrm{T}}$ is the control input, where δ_{ei}, δ_{ai}, and δ_{ri} represent the deflection of elevator, ailerons, and rudder, respectively, $\boldsymbol{g} = [0, 0, g_z]^{\mathrm{T}}$ is the gravity acceleration in inertia frame, $\boldsymbol{d}_{vi} \in \Re^3$ and $\boldsymbol{d}_{\omega i} \in \Re^3$ are the unknown bounded external disturbances, and $\boldsymbol{J}_i$ is the inertia tensor with the symmetric $x-z$ plane of which expression is

$$\boldsymbol{J}_i = \begin{bmatrix} J_{xi} & 0 & -J_{xzi} \\ 0 & J_{yi} & 0 \\ -J_{xzi} & 0 & J_{zi} \end{bmatrix}. \tag{5}$$

Besides, $\boldsymbol{R}_1(\boldsymbol{\varphi}_i) \in \text{SO}(3)$ is the rotation matrix transforming the body frame coordinates to inertial axis coordinates and the matrix $\boldsymbol{R}_2(\boldsymbol{\varphi}_i) \in \Re^{3\times 3}$ maps the time derivative of the Euler angles to the noninertial expression of the angular velocity. Both matrices are given as follows:

$$\boldsymbol{R}_1(\boldsymbol{\varphi}_i) = \begin{bmatrix} c_{\psi_i}c_{\theta_i} - s_{\psi_i}s_{\phi_i} + c_{\psi_i}s_{\theta_i}s_{\phi_i}s_{\psi_i}s_{\phi_i} + c_{\psi_i}s_{\theta_i}c_{\phi_i} \\ s_{\psi_i}c_{\theta_i} \quad c_{\psi_i}c_{\phi_i} + s_{\psi_i}s_{\theta_i}s_{\phi_i} - c_{\psi_i}s_{\phi_i} + s_{\psi_i}s_{\theta_i}c_{\phi_i} \\ -s_{\theta_i} \qquad c_{\theta_i}s_{\phi_i} \qquad c_{\theta_i}c_{\phi_i} \end{bmatrix}$$

$$\boldsymbol{R}_2(\boldsymbol{\varphi}_i) = \begin{bmatrix} 1 & 0 & -s_{\psi_i} \\ 0 & c_{\psi_i} & s_{\psi_i}c_{\theta_i} \\ 0 & -s_{\theta_i} & c_{\psi_i}c_{\theta_i} \end{bmatrix} \tag{6}$$

where s_a and c_a stand for $\sin(a)$ and $\cos(a)$ functions, respectively. The aerodynamics force $\boldsymbol{F}_i = [F_{Xi}, F_{Yi}, F_{Zi}]^{\mathrm{T}}$ and moment $\boldsymbol{N}_i = [F_{Li}, F_{Mi}, F_{Ni}]^{\mathrm{T}}$ are calculated by means of aerodynamic coefficients

$$\boldsymbol{F}_i = \bar{q}_i S_i \boldsymbol{R}_3^{-1}(\alpha_i, \beta_i)[-C_{Di}, C_{Yi}, -C_{Li}]^{\mathrm{T}} \tag{7}$$

$$\boldsymbol{N}_i = \bar{q}_i S_i [b_i C'_{li}, \bar{c}_i C'_{Mi}, b_i C'_{ni}]^{\mathrm{T}} \tag{8}$$

where $\alpha_i = \arctan(w_i/u_i)$ and $\beta_i = \arcsin(u_i/v_i)$ denote the attack angle and sideslip angle, respectively. The dynamic pressure $\bar{q}_i = \frac{1}{2}\rho V_i^2$ is a function of total velocity $V_i = \sqrt{u_i^2 + v_i^2 + w_i^2}$. Air density ρ, wingspan b_i, wing surface area S_i, and mean aerodynamic chord $\bar{c}_i$ are constant parameters. The transformation matrix $\boldsymbol{R}_3(\alpha_i, \beta_i)$ is

$$\boldsymbol{R}_3(\alpha_i, \beta_i) = \begin{bmatrix} c_{\alpha_i}c_{\beta_i} & s_{\beta_i} & s_{\alpha_i}c_{\beta_i} \\ -c_{\alpha_i}s_{\beta_i} & c_{\beta_i} & -s_{\alpha_i}s_{\beta_i} \\ -s_{\alpha_i} & 0 & c_{\alpha_i} \end{bmatrix}. \tag{9}$$

And C_{Di}, C_{Yi}, C_{Li}, C'_{li}, C'_{Mi}, and C'_{ni} are the dimensionless coefficients in force/moment expressions, of which corresponding detailed descriptions are shown in [32]. The control effectiveness matrix is defined as

$$\boldsymbol{C}(\boldsymbol{\delta}_i) = \begin{bmatrix} \bar{q}_i S_i b_i c_{l\delta_{ai}} & 0 & \bar{q}_i S_i b_i c_{l\delta_{ri}} \\ 0 & \bar{q}_i S_i \bar{c}_i c_{m\delta_{ei}} & 0 \\ \bar{q}_i S_i b_i c_{n\delta_{ai}} & 0 & \bar{q}_i S_i b_i c_{n\delta_{ri}} \end{bmatrix}. \tag{10}$$

C. Control-Oriented Model

According to [31] and [32], the whole system can be decomposed into two interconnected subsystems, i.e., translational kinematics (2) and rotational one (3), (4).

1) Translational Kinematics: From (2), the thrust is extracted and using the property $\boldsymbol{v}_i^{\mathrm{T}}\boldsymbol{S}(\boldsymbol{\omega}_i)\boldsymbol{v}_i = 0$, it holds that

$$\dot{V}_i = \frac{\boldsymbol{v}_i^{\mathrm{T}}\dot{\boldsymbol{v}}_i}{V_i} = \frac{u_i T_{xi}}{m_i V_i} + \frac{\boldsymbol{v}_i^{\mathrm{T}}}{V_i}\left(\boldsymbol{R}_1^{\mathrm{T}}(\boldsymbol{\varphi}_i)\,\boldsymbol{g} + \frac{\boldsymbol{F}_i}{m_i} + \boldsymbol{d}_{vi}\right) \tag{11}$$

which satisfies $V_{i,\min}(t) < V_i(t) < V_{i,\max}(t)\ \forall t \geq 0$.

During operation, the thrust possibly suffers from actuator faults, modeled by [33]

$$T_{xi} = \rho_{T_i} T_{xi0} + T_{xif} \tag{12}$$

where T_{xi0} is the designed control input, ρ_{T_i} is the unknown actuator efficiency factor satisfying $0 \leq \rho_{T_i} \leq 1$, and T_{xif} is the bounded unknown stuck fault or bias fault. Note that (12) implies the following four cases.

1) $\rho_{T_i} = 1$ and $T_{xif} = 0$. This means the fault-free case.
2) $0 < \rho_{T_i} < 1$ and $T_{xif} = 0$. This indicates the partial loss of effectiveness.
3) $\rho_{T_i} = 1$ and $T_{xif} \neq 0$. This indicates the bias fault.
4) $\rho_{T_i} = 0$ and $T_{xif} \neq 0$. This means that T_{xi} is stuck at the bounded time-varying function T_{xif}.

Moreover, note that the accurate information of $\boldsymbol{F}_i$ cannot be known a prior due to the coefficient uncertainties. In this sense, $\boldsymbol{F}_i$ is decomposed into a known component $\boldsymbol{F}_{i0}$ and an uncertain one $\Delta\boldsymbol{F}_i$ [9]. Thus, with the actuator faults and modeling uncertainties, the velocity kinematics is reformulated as

$$\dot{V}_i = \frac{u_i\rho_{T_i}T_{xi0}}{m_i V_i} + \frac{u_i T_{xif}}{m_i V_i} + \frac{\boldsymbol{v}_i^{\mathrm{T}}}{V_i}\left(\boldsymbol{R}_1^{\mathrm{T}}(\boldsymbol{\varphi}_i)\,\boldsymbol{g} + \frac{\boldsymbol{F}_{i0}}{m_i} + \frac{\Delta\boldsymbol{F}_i}{m_i} + \boldsymbol{d}_{vi}\right). \tag{13}$$

2) Rotational Kinematics: From (3) and (4), the dynamical attitude motion is rewritten as

$$\dot{\boldsymbol{\varphi}}_i = \boldsymbol{R}_2^{-1}(\boldsymbol{\varphi}_i)\,\boldsymbol{\omega}_i \tag{14}$$

$$\dot{\boldsymbol{\omega}}_i = \boldsymbol{J}_i^{-1}\boldsymbol{S}(\boldsymbol{J}_i\boldsymbol{\omega}_i) + \boldsymbol{J}_i^{-1}\boldsymbol{N}_i + \boldsymbol{J}_i^{-1}\boldsymbol{C}(\boldsymbol{\delta}_i)\,\boldsymbol{\delta}_i + \boldsymbol{d}_{\omega i} \tag{15}$$

which satisfies $-\boldsymbol{\varphi}_{i,\min}(t) < \boldsymbol{\varphi}_i(t) < \boldsymbol{\varphi}_{i,\max}(t)$ and $-\boldsymbol{\omega}_{i,\min}(t) < \boldsymbol{\omega}_i(t) < \boldsymbol{\omega}_{i,\max}(t)\ \forall t \geq 0$.

During flight, the flight control surfaces inevitably suffers from actuator faults, which are considered as [13]

$$\delta_{mi} = \rho_{\delta_{mi}}\delta_{mi0} + \delta_{mif} \tag{16}$$

where δ_{mi0} is the mth applied control input with $m = \{a, e, r\}$, $\rho_{\delta_{mi}}$ is the unknown actuator efficiency factor satisfying $0 \leq \rho_{\delta_{mi}} \leq 1$, and δ_{mif} is the bounded unknown stuck fault or bias fault. Consider that (16) satisfies the similar cases as (12) in the following.

1) $\rho_{\delta_{mi}} = 1$ and $\delta_{mif} = 0$. This refers to the fault-free case.
2) $0 < \rho_{\delta_{mi}} < 1$ and $\delta_{mif} = 0$. This means the partial loss of effectiveness.
3) $\rho_{\delta_{mi}} = 1$ and $\delta_{mif} \neq 0$. This indicates the bias fault.
4) $\rho_{\delta_{mi}} = 0$ and $\delta_{mif} \neq 0$. This means that δ_{mi} is stuck at bounded time-varying function δ_{mif}.

For the simplicity of presentation, the actuator fault model is formulated by

$$\boldsymbol{\delta}_i = \boldsymbol{\rho}_{\delta_i}\boldsymbol{\delta}_{i0} + \boldsymbol{\delta}_{if} \tag{17}$$

where $\boldsymbol{\delta}_{i0} = [\delta_{ai0}, \delta_{ei0}, \delta_{ri0}]^{\mathrm{T}}$, $\boldsymbol{\rho}_{\delta_i} = \mathrm{diag}\{\rho_{\delta_{ai}}, \rho_{\delta_{ei}}, \rho_{\delta_{ri}}\}$, and $\boldsymbol{\delta}_{if} = [\delta_{aif}, \delta_{eif}, \delta_{rif}]^{\mathrm{T}}$.

And meanwhile, considering the coefficient uncertainties, $\boldsymbol{J}_i^{-1}\boldsymbol{S}(\boldsymbol{J}_i\boldsymbol{\omega}_i)$ is decomposed into a known component $\boldsymbol{J}_{i0}^{-1}\boldsymbol{S}(\boldsymbol{J}_{i0}\boldsymbol{\omega}_i)$ and an uncertain one $\Delta\boldsymbol{J}_i^{-1}\boldsymbol{S}(\boldsymbol{J}_i\boldsymbol{\omega}_i)$. Similarly, $\boldsymbol{J}_i^{-1}\boldsymbol{N}_i$ is composed by a known part $\boldsymbol{J}_{i0}^{-1}\boldsymbol{N}_{i0}$ and an uncertain one $\Delta\boldsymbol{J}_i^{-1}\boldsymbol{N}_i$. Also, $\boldsymbol{J}_i^{-1}\boldsymbol{C}(\boldsymbol{\delta}_i)$ consists of a known component $\boldsymbol{J}_{i0}^{-1}\boldsymbol{C}_0(\boldsymbol{\delta}_i)$ and an uncertain one $\Delta\boldsymbol{J}_i^{-1}\boldsymbol{C}(\boldsymbol{\delta}_i)$. Accordingly, in the presence of actuator faults and modeling uncertainties, the dynamic model of the angular velocity can be formulated by

$$\begin{aligned}\dot{\boldsymbol{\omega}}_i = {} & \boldsymbol{J}_{i0}^{-1}\boldsymbol{S}(\boldsymbol{J}_{i0}\boldsymbol{\omega}_i) + \boldsymbol{J}_{i0}^{-1}\boldsymbol{N}_{i0} + \boldsymbol{J}_{i0}^{-1}\boldsymbol{C}_0(\boldsymbol{\delta}_i)\,\boldsymbol{\rho}_{\delta_i}\boldsymbol{\delta}_{i0} \\ & + \boldsymbol{\Delta}_{\omega i} + \boldsymbol{d}_{\omega i}\end{aligned} \tag{18}$$

where $\boldsymbol{\Delta}_{\omega i} = \Delta\boldsymbol{J}_i^{-1}\boldsymbol{S}(\boldsymbol{J}_i\boldsymbol{\omega}_i) + \Delta\boldsymbol{J}_i^{-1}\boldsymbol{N}_i + \Delta\boldsymbol{J}_i^{-1}\boldsymbol{C}(\boldsymbol{\delta}_i)\boldsymbol{\delta}_i + \boldsymbol{J}_{i0}^{-1}\boldsymbol{C}_0(\boldsymbol{\delta}_i)\boldsymbol{\delta}_{if}$ is the lumped uncertainties induced by actuator faults and modeling uncertainties.

Assumption 2: For all $t > 0$, it is supposed that $\|\Delta\boldsymbol{J}_i^{-1}\boldsymbol{C}(\boldsymbol{\delta}_i)\boldsymbol{\rho}_{\delta_i}(\boldsymbol{J}_{i0}^{-1}\boldsymbol{C}_0(\boldsymbol{\delta}_i))^{-1}\|_\infty < 1$ and $\partial\boldsymbol{\Delta}_{\omega i}/\partial\boldsymbol{\delta}_{i0} + \boldsymbol{J}_{i0}^{-1}\boldsymbol{C}_0(\boldsymbol{\delta}_i)\boldsymbol{\rho}_{\delta_i} \neq 0$.

Assumption 3: There exists a constant $g_{i,\min}$ such that $\lambda_{\min}(\boldsymbol{J}_{i0}^{-1}\boldsymbol{C}_0(\boldsymbol{\delta}_i)\boldsymbol{\rho}_{\delta_i}(\boldsymbol{J}_{i0}^{-1}\boldsymbol{C}_0(\boldsymbol{\delta}_i))^{\mathrm{T}}) \geq g_{i,\min} > 0$.

Remark 1: Assumption 2 imposes the controllability condition to the model (18), which guarantees the existence of the controller $\boldsymbol{\delta}_{i0}$. While the Assumption 2 is essential so that the control signal $\boldsymbol{\delta}_{i0}$ dominates the uncertain vector $(\boldsymbol{J}_{i0}^{-1}\boldsymbol{C}_{i0}(\boldsymbol{\delta}_i)\boldsymbol{\rho}_{\delta_i} + \Delta\boldsymbol{J}_i^{-1}\boldsymbol{C}(\boldsymbol{\delta}_i))\boldsymbol{\delta}_{i0}$. Similar assumptions can be found in [7], [13], and [34]. Moreover, from Assumption 3, $g_{i,\min}$ is just used for analysis and not required *a priori*.

Remark 2: Considering that $\boldsymbol{\Delta}_{\omega i}$ involves the control signal $\boldsymbol{\delta}_{i0}$, if neural networks are used to approximate $\boldsymbol{\Delta}_{\omega i}$, the algebraic loops inevitably exist. To break the algebraic loops, the low-pass filter technique is employed to filter $\boldsymbol{\delta}_{i0}$ [33]. We obtain $\boldsymbol{\Delta}_{\omega i} = \boldsymbol{\Delta}'_{\omega i} + \boldsymbol{l}_{\omega i}$, where $\boldsymbol{l}_{\omega i} \in \Re^3$ is the filtering error.

D. Neural Network Approximation

As the universal approximation property, the radial basis function neural networks (RBFNNs) are employed in this article to compensate the modeling uncertainties [35], [36]. Denote $\boldsymbol{\Theta}_{vi} = [\boldsymbol{v}_i^{\mathrm{T}}, \boldsymbol{\varphi}_i^{\mathrm{T}}, \boldsymbol{\omega}_i^{\mathrm{T}}, \boldsymbol{\delta}_{i0}^{\mathrm{T}}]^{\mathrm{T}} \in \Re^{12}$ and $\boldsymbol{\Theta}_{\omega i} = [\boldsymbol{v}_i^{\mathrm{T}}, \boldsymbol{\varphi}_i^{\mathrm{T}}, \boldsymbol{\omega}_i^{\mathrm{T}}, \boldsymbol{\delta}_{i0}^{\mathrm{T}}]^{\mathrm{T}} \in \Re^{12}$. For unknown continuous terms $\boldsymbol{\Delta}_{vi}(\boldsymbol{\Theta}_{vi}) = [\Delta_{vi1}, \Delta_{vi2}, \Delta_{vi3}]^{\mathrm{T}}$ and $\boldsymbol{\Delta}'_{\omega i}(\boldsymbol{\Theta}_{\omega i}) = [\Delta'_{\omega i1}, \Delta'_{\omega i2}, \Delta'_{\omega i3}]^{\mathrm{T}}$, there exist RBFNNs such that

$$\begin{aligned}\Delta_{vil}(\boldsymbol{\Theta}_{vi}) &= \boldsymbol{W}_{vil}^{*\mathrm{T}}\boldsymbol{\varsigma}_{vil}(\boldsymbol{\Theta}_{vi}) + \tau_{vil}(\boldsymbol{\Theta}_{vi}) \\ \Delta'_{\omega il}(\boldsymbol{\Theta}_{\omega i}) &= \boldsymbol{W}_{\omega il}^{*\mathrm{T}}\boldsymbol{\varsigma}_{\omega il}(\boldsymbol{\Theta}_{\omega i}) + \tau_{\omega il}(\boldsymbol{\Theta}_{\omega i})\end{aligned} \tag{19}$$

where $l = 1, 2, 3$, $\tau_{vil}(\boldsymbol{\Theta}_{vi}) \in \Re$ and $\tau_{\omega il}(\boldsymbol{\Theta}_{\omega i}) \in \Re$ are the bounded approximation errors. $\boldsymbol{W}_{vil}^* \in \Re^{M\times 1}$ and $\boldsymbol{W}_{\omega il}^* \in \Re^{M\times 1}$ are ideal weight matrixes with M nodes. $\boldsymbol{\varsigma}_{vil}(\boldsymbol{\Theta}_{vi}) = [\varsigma_{vil}^1(\boldsymbol{\Theta}_{vi}), \ldots, \varsigma_{vil}^M(\boldsymbol{\Theta}_{vi})]^{\mathrm{T}} \in \Re^M$ and $\boldsymbol{\varsigma}_{\omega il}(\boldsymbol{\Theta}_{\omega i}) = [\varsigma_{\omega il}^1(\boldsymbol{\Theta}_{\omega i}), \ldots, \varsigma_{\omega il}^M(\boldsymbol{\Theta}_{\omega i})]^{\mathrm{T}} \in \Re^M$ are known vectors consisted Gaussian basis functions $\varsigma_{vil}^n(\boldsymbol{\Theta}_{vi})$ and $\varsigma_{\omega il}^n(\boldsymbol{\Theta}_{\omega i})$, $n = 1, \ldots, M$, commonly selected as the following exponential form:

$$\begin{aligned}\varsigma_{vij}^n(\boldsymbol{\Theta}_{vi}) &= \exp\left[-\frac{(\boldsymbol{\Theta}_{vi} - \boldsymbol{\Upsilon}_{vi})^{\mathrm{T}}(\boldsymbol{\Theta}_{vi} - \boldsymbol{\Upsilon}_{vi})}{\kappa_{vi}^2}\right] \\ \varsigma_{\omega ij}^n(\boldsymbol{\Theta}_{\omega i}) &= \exp\left[-\frac{(\boldsymbol{\Theta}_{\omega i} - \boldsymbol{\Upsilon}_{\omega i})^{\mathrm{T}}(\boldsymbol{\Theta}_{\omega i} - \boldsymbol{\Upsilon}_{\omega i})}{\kappa_{\omega i}^2}\right]\end{aligned} \tag{20}$$

where $\boldsymbol{\Upsilon}_{vi} \in \Re^{12}$ and $\boldsymbol{\Upsilon}_{\omega i} \in \Re^{12}$ are the centers of the receptive filed, and κ_{vi} and $\kappa_{\omega i}$ are the width of the Gaussian basis functions.

E. Control Objective

Given the velocity reference V_r and attitude reference $\boldsymbol{\varphi}_r$, the goal is to design the cooperative distributed fixed-time tracking controller such that

1) All the closed-loop signals remain bounded and the velocity and attitude tracking errors for each UAV are semiglobally uniformly ultimately bounded (SGUUB) within fixed time in spite of actuator faults, modeling uncertainties, and external disturbances.
2) The performances of velocity and attitude preserve certain constraints at all time.

Assumption 4: The designed parameters $V_{i,\min}$, $V_{i,\max}$, $\boldsymbol{\varphi}_{i,\min}$, $\boldsymbol{\varphi}_{i,\max}$, $\boldsymbol{\omega}_{i,\min}$, and $\boldsymbol{\omega}_{i,\max}$ and their time-derivatives up to second order are continuous and bounded.

For the convenience of derivation, the following lemmas are needed.

Lemma 1 [37]: Consider the system

$$\dot{\boldsymbol{x}}(t) = f(\boldsymbol{x}(t)),\ \boldsymbol{x}(0) = \boldsymbol{x}_0. \tag{21}$$

Suppose that there exists constants $\alpha > 0, \beta > 0, p > 1, 0 < q < 1$, and $0 < \eta < \infty$ such that

$$\dot{V}(\boldsymbol{x}) \leq -\alpha V^p(\boldsymbol{x}) - \beta V^q(\boldsymbol{x}) + \eta. \tag{22}$$

Then, the system (21) is practically fixed-time stable. The settling time T is presented as $T \leq T_{\max} := \frac{1}{\alpha\phi(p-1)} + \frac{1}{\beta\phi(1-q)}$ with $0 < \phi < 1$. The convergence neighborhood is given by $\boldsymbol{x} \in \{V(\boldsymbol{x}) \leq \min\{(\frac{\eta}{(1-\phi)\alpha})^{\frac{1}{p}}, (\frac{\eta}{(1-\phi)\beta})^{\frac{1}{q}}\}\}$.

Lemma 2 [38]: For any scalars $\varepsilon > 0$, $z \in \Re$, the following equation holds: $0 \leq |z| - \frac{z^2}{\sqrt{z^2+\varepsilon}} \leq \sqrt{\varepsilon}$.

Lemma 3 [39]: For any scalars $\varepsilon > 0$, $\vartheta \in \Re$, $0 \leq |\vartheta| - \vartheta \tanh(\frac{\vartheta}{\varepsilon}) \leq 0.2785\varepsilon$ holds.

Lemma 4 [40]: For positive constants b_1, b_2 and b_3, it follows that

$$|x|^{b_1}|y|^{b_2} \leq \frac{b_1}{b_1+b_2}b_3|x|^{b_1+b_2} + \frac{b_2}{b_1+b_2}b_3^{-\frac{b_1}{b_2}}|y|^{b_1+b_2}$$

where x and y are real variables.

III. Cooperative Distributed Fixed-Time Controller Design

A. State Transformation

The system transformation is developed to transform the original constrained system (13), (14), and (18) into the unconstrained ones, whose stability can guarantee the full-state constraints.

1) Translational Kinematics: Let $\tilde{V}_i = V_i - V_r$ represent the tracking error of velocity for each UAV with V_r piecewise continuously differentiable.

Definition 1: Velocity tracking is said to guarantee $-F_{vi1}(t) < \tilde{V}_i(t) < F_{vi2}(t)$ if for any given bounded initial condition satisfying $-F_{vi1}(0) < \tilde{V}_i(0) < F_{vi2}(0)$. If there exists

$$\xi_{vi} = \frac{\tilde{V}_i}{\left(F_{vi1} + \tilde{V}_i\right)\left(F_{vi2} - \tilde{V}_i\right)} \tag{23}$$

the constraint of $\tilde{V}_i$ can be ensured as ξ_{vi} is bounded $\forall t \geq 0$.

From (23), taking the derivative of ξ_{vi} gives

$$\dot{\xi}_{vi} = \eta_{vi}\dot{\tilde{V}}_i(t) + \mu_{vi} \tag{24}$$

where

$$\eta_{vi} = \frac{F_{vi1}F_{vi2} + \tilde{V}_i^2}{\left(F_{vi1} + \tilde{V}_i\right)^2\left(F_{vi2} - \tilde{V}_i\right)^2}$$

$$\mu_{vi} = \frac{\left[\dot{F}_{vi1}F_{vi2} + F_{vi1}\dot{F}_{vi2} + (\dot{F}_{vi2} - \dot{F}_{vi1})\tilde{V}_i\right]\tilde{V}_i}{\left(F_{vi1} + \tilde{V}_i\right)^2\left(F_{vi2} - \tilde{V}_i\right)^2}.$$

2) Rotational Kinematics: Let $\boldsymbol{e}_{\varphi i}$ denote the error vector that specifies synchronization attitude for each UAV with $\boldsymbol{\varphi}_r$ piecewise continuously differentiable

$$\boldsymbol{e}_{\varphi i} = \lambda_{i1}\tilde{\boldsymbol{\varphi}}_i + \lambda_{i2}\sum_{j\in\mathcal{N}_i} a_{ij}\left(\tilde{\boldsymbol{\varphi}}_i - \tilde{\boldsymbol{\varphi}}_j\right) \tag{25}$$

where $\tilde{\boldsymbol{\varphi}}_i = \boldsymbol{\varphi}_i - \boldsymbol{\varphi}_r$, $\tilde{\boldsymbol{\varphi}}_j = \boldsymbol{\varphi}_j - \boldsymbol{\varphi}_r$, and λ_{i1} and λ_{i2} are positive design parameters.

Definition 2: Synchronization attitude tracking is identified with $-F_{\varphi il1}(t) < e_{\varphi il}(t) < F_{\varphi il2}(t)$ for $l = 1, 2, 3$ if for any given bounded initial condition satisfying $-F_{\varphi il1}(0) < e_{\varphi il}(0) < F_{\varphi il2}(0)$. If there exists

$$\xi_{\varphi il} = \frac{e_{\varphi il}}{\left(F_{\varphi il1} + e_{\varphi il}\right)\left(F_{\varphi il2} - e_{\varphi il}\right)} \tag{26}$$

the constraint on $e_{\varphi il}$ can be guaranteed if $\xi_{\varphi il}$ is bounded $\forall t \geq 0$.

Take the time derivative of $\xi_{\varphi il}$ along (26) as

$$\dot{\xi}_{\varphi il} = \eta_{\varphi il}\dot{e}_{\varphi il} + \mu_{\varphi il} \tag{27}$$

where

$$\eta_{\varphi il} = \frac{F_{\varphi il1}F_{\varphi il2} + {e_{\varphi il}}^2}{\left(F_{\varphi il1} + e_{\varphi il}\right)^2\left(F_{\varphi il2} - e_{\varphi il}\right)^2}$$

$$\mu_{\varphi il} = \frac{\left[\dot{F}_{\varphi il1}F_{\varphi il2} + F_{\varphi il1}\dot{F}_{\varphi il2} + (\dot{F}_{\varphi il2} - \dot{F}_{\varphi il1})e_{\varphi il}\right]e_{\varphi il}}{\left(F_{\varphi il1} + e_{\varphi il}\right)^2\left(F_{\varphi il2} - e_{\varphi il}\right)^2}.$$

We have $\boldsymbol{\xi}_{\varphi i} = [\xi_{\varphi i1}, \xi_{\varphi i2}, \xi_{\varphi i3}]^{\mathrm{T}}$, $\boldsymbol{\mu}_{\varphi i} = [\mu_{\varphi i1}, \mu_{\varphi i2}, \mu_{\varphi i3}]^{\mathrm{T}}$, and $\boldsymbol{\eta}_{\varphi i} = \mathrm{diag}\{\eta_{\varphi i1}, \eta_{\varphi i2}, \eta_{\varphi i3}\}$.

Definition 3: The time-varying constraint on $\boldsymbol{\omega}_i$ is never transgressed, that is, $-F_{\omega il1}(t) < \omega_{il}(t) < F_{\omega il2}(t)$ for $l = 1, 2, 3$ if for any given bounded initial state satisfying $-F_{\omega il1}(0) < \omega_{il}(0) < F_{\omega il2}(0)$. If there exists

$$\xi_{\omega il} = \frac{\omega_{il}}{\left(F_{\omega il1} + \omega_{il}\right)\left(F_{\omega il2} - \omega_{il}\right)} \tag{28}$$

the constrained problem of ω_{il} equals to ensure the boundedness of $\xi_{\omega il}$ $\forall t \geq 0$.

From (28), taking the time derivative of $\xi_{\omega il}$ gives

$$\dot{\xi}_{\omega il} = \eta_{\omega il}\dot{\omega}_{il} + \mu_{\omega il} \tag{29}$$

where

$$\eta_{\omega il} = \frac{F_{\omega il1}F_{\omega il2} + \omega_{il}^2}{\left(F_{\omega il1} + \omega_{il}\right)^2\left(F_{\omega il2} - \omega_{il}\right)^2}$$

$$\mu_{\omega il} = \frac{\left[\dot{F}_{\omega il1}F_{\omega il2} + F_{\omega il1}\dot{F}_{\omega il2} + (\dot{F}_{\omega il2} - \dot{F}_{\omega il1})\omega_{il}\right]\omega_{il}}{\left(F_{\omega il1} + \omega_{il}\right)^2\left(F_{\omega il2} - \omega_{il}\right)^2}$$

We define $\boldsymbol{\xi}_{\omega i} = [\xi_{\omega i1}, \xi_{\omega i2}, \xi_{\omega i3}]^{\mathrm{T}}$, $\boldsymbol{\mu}_{\omega i} = [\mu_{\omega i1}, \mu_{\omega i2}, \mu_{\omega i3}]^{\mathrm{T}}$, and $\boldsymbol{\eta}_{\omega i} = \mathrm{diag}\{\eta_{\omega i1}, \eta_{\omega i2}, \eta_{\omega i3}\}$.

Remark 3: $F_{vi1}(t)$, $F_{vi2}(t)$, $F_{\varphi il1}(t)$, $F_{\varphi il2}(t)$, $F_{\omega il1}(t)$, and $F_{\omega il2}(t)$ are utilized to described the time-varying constraints for $\tilde{V}_i$, $e_{\varphi il}$, and ω_{il}, respectively. Note that $F_{vi1}(t)$, $F_{vi2}(t)$, $F_{\varphi il1}(t)$, $F_{\varphi il2}(t)$, $F_{\omega il1}(t)$, and $F_{\omega il2}(t)$ are strictly positive smooth functions. More details on the properties of the constrained problem described by (23), (26), and (28) can refer to the illustration example in [25]. Based on Definitions 1–3, new unconstrained subsystems (23), (26), and (28) for translational and rotational dynamics are obtained, which are guaranteed to be bounded.

B. Controller Design

Following the double-layer control structure, the translational and rotational controller design are proposed, respectively. Hereafter, the design of T_{xi0} and $\boldsymbol{\delta}_{i0}$ are given.

1) Translational Kinematics: To achieve the control objective, we employ the dynamic controller T_{xi0} (see Algorithm 1)

$$T_{xi0} = -\frac{\alpha_{vi}\hat{\beta}_{vi}}{\zeta_{vi}}\tanh\left(\frac{\xi_{vi}\eta_{vi}\alpha_{vi}\hat{\beta}_{vi}}{\varepsilon_{vi}}\right) - \hat{g}_{vi}\tanh\left(\frac{\xi_{vi}\eta_{vi}\hat{g}_{vi}\zeta_{vi}}{\varepsilon_{vi}}\right) \tag{30}$$

where $\alpha_{vi} = \frac{c_{vi1}}{\eta_{vi}}\mathrm{sig}(\xi_{vi})^{2p_v-1} + \frac{c_{vi2}}{\eta_{vi}}\mathrm{sig}(\xi_{vi})^{2q_v-1} + \frac{\hat{\Phi}_{vi}\boldsymbol{v}_i^{\mathrm{T}}\boldsymbol{\Xi}_{vi}}{2h_{vi1}^2{V_i}^2} + \frac{\boldsymbol{v}_i^{\mathrm{T}}}{V_i}(\boldsymbol{R}_1^{\mathrm{T}}\boldsymbol{g} + \frac{\boldsymbol{F}_{i0}}{m_i}) + \frac{\xi_{vi}\eta_{vi}\boldsymbol{v}_i^{\mathrm{T}}\boldsymbol{v}_i}{2h_{vi2}^2V_i^2} - \dot{V}_r + \frac{\mu_{vi}}{\eta_{vi}}$ with $p_v > 1$, $0 < q_v < 1$, $\boldsymbol{\Xi}_{vi} = \xi_{vi}\eta_{vi}[v_{i1}\boldsymbol{\varsigma}_{vi1}^{\mathrm{T}}\boldsymbol{\varsigma}_{vi1}, v_{i2}\boldsymbol{\varsigma}_{vi2}^{\mathrm{T}}\boldsymbol{\varsigma}_{vi2}, v_{i3}\boldsymbol{\varsigma}_{vi3}^{\mathrm{T}}\boldsymbol{\varsigma}_{vi3}]^{\mathrm{T}}$. The adaptive parameters $\hat{\Phi}_{vi}$, $\hat{g}_{vi}$, and $\hat{\beta}_{vi}$ are updated by

$$\dot{\hat{\Phi}}_{vi} = \frac{\gamma_{vi1}\xi_{vi}\eta_{vi}\boldsymbol{v}_i^{\mathrm{T}}\boldsymbol{\Xi}_{vi}}{2h_{vi1}^2V_i} - \gamma_{vi1}\sigma_{vi1}\hat{\Phi}_{vi} \tag{31}$$

$$\dot{\hat{g}}_{vi} = \gamma_{vi2}\left|\xi_{vi}\eta_{vi}\right|\zeta_{vi} - \gamma_{vi2}\sigma_{vi2}\hat{g}_{vi} \tag{32}$$

$$\dot{\hat{\beta}}_{vi} = \gamma_{vi3}\xi_{vi}\eta_{vi}\alpha_{vi} - \gamma_{vi3}\sigma_{vi3}\hat{\beta}_{vi} \tag{33}$$

Algorithm 1: Design the Distributed Control Protocol T_{xi0}.

Input: The parameters F_{vi1} and F_{vi2} in state transformation (23); the parameters γ_{vi1}, γ_{vi2}, γ_{vi3}, σ_{vi1}, σ_{vi2}, σ_{vi3}, and h_{vi1} in adaptive laws (31)–(33); the parameters c_{vi1}, c_{vi2}, h_{vi2}, and ε_{vi} in the control protocol (30).

Output: The distributed control protocol (30).

1: **Step 1:** Solve the velocity constraints to obtain the state transformation (23).
2: **Step 2:** Use the RBFNN (19) to approximate the modeling uncertainties, and acquire the adaptive law (31).
3: **Step 3:** Introduce $\beta_{vi} = 1/\rho_{T_i}$ and $g_{vi} = \beta_{vi} \sup_{t\geq 0} T_{xif}$ to compensate for the actuator faults, and obtain the adaptive laws (32) and (33).
4: **Step 4:** Select the parameters c_{vi1}, c_{vi2}, h_{vi2}, and ε_{vi}, and integrate the adaptive laws (31)–(33) into the control protocol (30).

where h_{vi1}, h_{vi2}, γ_{vi1}, γ_{vi2}, γ_{vi3}, σ_{vi1}, σ_{vi2}, σ_{vi3}, and ε_{vi} are positive design parameters.

Theorem 1: Consider the translational kinematics (13) composed by the adaptive controller (30) and parameter adaptation laws (31)–(33). Let Assumptions 4 hold. There exist positive parameters $c_{vi1}, c_{vi2}, \varepsilon_{vi}, h_{vi1}, h_{vi2}, \gamma_{vi1}, \gamma_{vi2}, \gamma_{vi3}, \sigma_{vi1}, \sigma_{vi2}$, and σ_{vi3} $(i = 1, 2, \ldots, N)$, such that the following are satisfied:

1) all signals of the translational subsystem are SGUUB in the presence of actuator faults, modeling uncertainties, and external disturbances;
2) velocity tracking error $\tilde{V}_i$ satisfies $\lim_{t\to T_{\max,v}} |\tilde{V}_i| \leq \mu_{vi}$ with $\mu_{vi} > 0$ a constant;
3) the required velocity constraint for the translational subsystem is guaranteed $\forall t \geq 0$.

Proof: See Appendix A.

2) Rotational Kinematics: To obtain the control objective, we propose the dynamic controller $\boldsymbol{\delta}_{i0}$ (see Algorithm 2)

$$\boldsymbol{\delta}_{i0} = -\left(\boldsymbol{J}_{i0}^{-1}\boldsymbol{C}_0\right)^{\mathrm{T}}\boldsymbol{\eta}_{\omega i}^{-1}\frac{\boldsymbol{e}_{\omega i}\hat{\beta}_{\omega i}^2\boldsymbol{\zeta}_{\omega i}^{\mathrm{T}}\boldsymbol{\zeta}_{\omega i}}{\sqrt{\hat{\beta}_{\omega i}^2\boldsymbol{e}_{\omega i}^{\mathrm{T}}\boldsymbol{e}_{\omega i}\boldsymbol{\zeta}_{\omega i}^{\mathrm{T}}\boldsymbol{\zeta}_{\omega i} + \varepsilon_{\omega i}}} \tag{34}$$

where $\boldsymbol{\zeta}_{\omega i} = \boldsymbol{K}_{4i}\boldsymbol{e}_{\omega i}\|\boldsymbol{e}_{\omega i}\|^{2p_\varphi - 2} + \boldsymbol{K}_{5i}\boldsymbol{e}_{\omega i}\|\boldsymbol{e}_{\omega i}\|^{2q_\varphi - 2} + \lambda_i\boldsymbol{K}_{1i}^{\mathrm{T}}(\boldsymbol{R}_2^{-1})^{\mathrm{T}}\boldsymbol{\eta}_{\varphi i}^{\mathrm{T}}\boldsymbol{\xi}_{\varphi i} + \boldsymbol{\eta}_{\omega i}\boldsymbol{J}_{i0}^{-1}\boldsymbol{S}(\boldsymbol{J}_{i0}\boldsymbol{\omega}_i) + \boldsymbol{\eta}_{\omega i}\boldsymbol{J}_{i0}^{-1}\boldsymbol{N}_{i0} + \frac{\hat{\Phi}_{\omega i}\boldsymbol{\eta}_{\omega i}\boldsymbol{\Xi}_{\omega i}}{2h_{\omega i1}^2} + \frac{\boldsymbol{\eta}_{\omega i}\boldsymbol{\eta}_{\omega i}^{\mathrm{T}}\boldsymbol{e}_{\omega i}}{2h_{\omega i2}^2} + \boldsymbol{\mu}_{\omega i} - \dot{\boldsymbol{\xi}}_{\omega di}$ with $p_\varphi > 1, 0 < q_\varphi < 1$, $\boldsymbol{\Xi}_{\omega i} = [e_{\omega i1}\eta_{\omega i1}\boldsymbol{\varsigma}_{\omega i1}^{\mathrm{T}}\boldsymbol{\varsigma}_{\omega i1}, e_{\omega i2}\eta_{\omega i2}\boldsymbol{\varsigma}_{\omega i2}^{\mathrm{T}}\boldsymbol{\varsigma}_{\omega i2}, e_{\omega i3}\eta_{\omega i3}\boldsymbol{\varsigma}_{\omega i3}^{\mathrm{T}}\boldsymbol{\varsigma}_{\omega i3}]^{\mathrm{T}}$, $\lambda_i = \lambda_{i1} + \lambda_{i2}\sum_{j\in\mathcal{N}_i} a_{ij}$. The adaptive parameters $\hat{\Phi}_{\omega i}$ and $\hat{\beta}_{\omega i}$ are updated by

$$\dot{\hat{\Phi}}_{\omega i} = \gamma_{\omega i1}\frac{\boldsymbol{e}_{\omega i}^{\mathrm{T}}\boldsymbol{\eta}_{\omega i}\boldsymbol{\Xi}_{\omega i}}{2h_{\omega i1}^2} - \sigma_{\omega i1}\gamma_{\omega i1}\hat{\Phi}_{\omega i} \tag{35}$$

$$\dot{\hat{\beta}}_{\omega i} = \gamma_{\omega i2}\boldsymbol{e}_{\omega i}^{\mathrm{T}}\boldsymbol{\zeta}_{\omega i} - \sigma_{\omega i2}\gamma_{\omega i2}\hat{\beta}_{\omega i} \tag{36}$$

where $h_{\omega i1}$, $h_{\omega i2}$, $\gamma_{\omega i1}$, $\gamma_{\omega i2}$, $\sigma_{\omega i1}$, $\sigma_{\omega i2}$, and $\varepsilon_{\omega i}$ are positive design parameters.

Theorem 2: Consider the rotational kinematics (14) and (18) composed by the controller (34) and adaptation laws (35) and (36). Let Assumptions 1–4 hold. There exist positive parameters $\boldsymbol{K}_{2i}, \boldsymbol{K}_{3i}, \boldsymbol{K}_{4i}, \boldsymbol{K}_{5i}, \varepsilon_{\omega i}, h_{\omega i1}, h_{\omega i2}, \gamma_{\omega i1}, \gamma_{\omega i2}$, and $\sigma_{\omega i1}, \sigma_{\omega i2}$ $(i = 1, 2, \ldots, N)$ such that the following are satisfied:

Algorithm 2: Design the Distributed Control Protocol $\boldsymbol{\delta}_{i0}$.

Input: The parameters $F_{\varphi il1}$, $F_{\varphi il2}$, $F_{\omega il1}$ and $F_{\omega il2}$ in state transformations (26) and (28); the parameters $\gamma_{\omega i1}$, $\gamma_{\omega i2}$, $\sigma_{\omega i1}$, $\sigma_{\omega i2}$ and $h_{\omega i1}$ in adaptive laws (35) and (36); the parameters $\boldsymbol{K}_{1i}$, $\boldsymbol{K}_{2i}$, and $\boldsymbol{K}_{3i}$ in virtual control (54); the parameters $\boldsymbol{K}_{4i}$, $\boldsymbol{K}_{5i}$, $h_{\omega i2}$, and $\varepsilon_{\omega i}$ in the control protocol (34).

Output: The distributed control protocol (34).

1: **Step 1:** Solve the attitude and angular velocity constraints to obtain the state transformations (26) and (28).
2: **Step 2:** Choose the parameters $\boldsymbol{K}_{1i}$, $\boldsymbol{K}_{2i}$ and $\boldsymbol{K}_{3i}$, and propose the virtual control (54).
3: **Step 3:** Use RBFNN (19) to approximate the modeling uncertainties, and acquire the adaptive law (35).
4: **Step 4:** Introduce $\beta_{\omega i} = 1/g_{\omega i}$ and $g_{\omega i} = \inf_{t\geq 0} \lambda_{\min}(\boldsymbol{J}_{i0}^{-1}\boldsymbol{C}_0(\boldsymbol{\delta}_i)\boldsymbol{\rho}_{\delta_i}(\boldsymbol{J}_{i0}^{-1}\boldsymbol{C}_0(\boldsymbol{\delta}_i))^{\mathrm{T}})$ to compensate for the actuator faults, and obtain the adaptive law (36).
5: **Step 5:** Choose the parameters $\boldsymbol{K}_{4i}$, $\boldsymbol{K}_{5i}$, $h_{\omega i2}$, and $\varepsilon_{\omega i}$, and integrate the adaptive laws (35) and (36) into the control protocol (34).

1) all signals of the rotational subsystem are SGUUB in spite of actuator faults, modeling uncertainties, and external disturbances;
2) attitude synchronization tracking error $\boldsymbol{e}_{\varphi i}$ achieves that $\lim_{t\to T_{\max,\varphi}} \|\boldsymbol{e}_{\varphi i}\| \leq \mu_{\varphi i}$ with $\mu_{\varphi i} > 0$ a constant;
3) the involved attitude constraints for rotational subsystem are guaranteed $\forall t \geq 0$;

Proof: See Appendix B.

Remark 4: By running the distributed control algorithm in parallel for each UAV, the proposed distributed control structure optimizes the time complexity, compared with the centralized control with an integral control algorithm for all UAVs [2]. Besides, note that only three scalar parameter adaptation laws (31)–(33) for translational dynamics and two scalar parameter adaptation laws (35), (36) for rotational dynamics are involved in our control design to deal with the actuator faults, modeling uncertainties, and disturbances, which makes it simpler than vector-based adaptation laws in backstepping control for UAVs [7]. In addition, our proposed fixed-time control owns the superiority in terms of convergence time, where the time convergence is independent of the initial condition. That is, the proposed fixed-time control can effectively shorten the execution time, which is comparable to time complexity of asymptotic controls and finite-time controls proposed for UAVs [13]–[15], [27]–[29], [31], [32].

Remark 5: The network-induced errors and actuator faults are effectively handled with the help of bound estimations for parameters $\beta_{vi} = 1/\rho_{T_i}$, $g_{vi} = \beta_{vi}\sup_{t\geq 0} T_{xif}$ in translational control protocol, and $\beta_{\omega i} = 1/g_{\omega i}$, $g_{\omega i} = \inf_{t\geq 0}\lambda_{\min}(\boldsymbol{J}_{i0}^{-1}\boldsymbol{C}_0(\boldsymbol{\delta}_i)\boldsymbol{\rho}_{\delta i}(\boldsymbol{J}_{i0}^{-1}\boldsymbol{C}_0(\boldsymbol{\delta}_i))^{\mathrm{T}})$ in the rotational control design. Further, we employ the smooth function $\vartheta\tanh(\frac{\vartheta}{\varepsilon})$ in design of T_{xi0} in (30), and function $\frac{z^2}{\sqrt{z^2+\varepsilon}}$ when designing $\boldsymbol{\delta}_{i0}$ in (34).

IV. Experimental and Simulation Validation

To demonstrate the feasibility of the proposed controller, the experimental validation is carried out based on the Links-RT

Fig. 1. Experiment prototype of the Links-RT UAV platform.

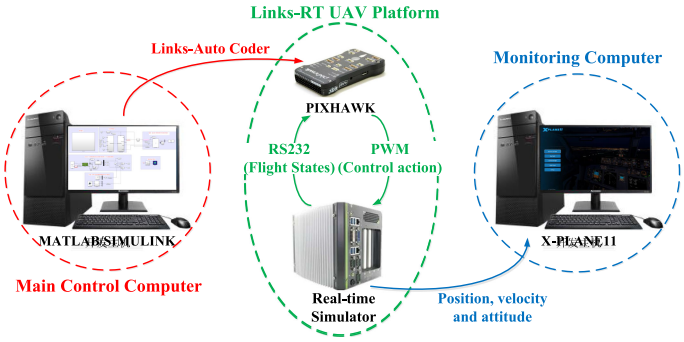

Fig. 2. Relationship between functional units.

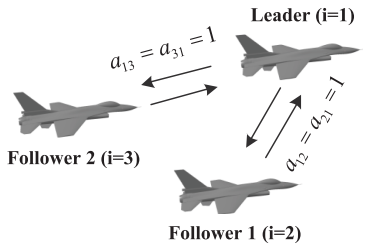

Fig. 3. Communication topology.

UAV Platform (supported by Beijing Links Company, Ltd.). The experiment setup and relationship between functional units are depicted in Figs. 1 and 2. The proposed controller is first implemented in MATLAB. Then, the code generation by Links-Auto Coder is used to convert the MATLAB language into C code, which is downloaded by Pixhawk. The Pixhawk is responsible for executing the proposed control algorithm with a sampling time of 2 ms and generating pulsewidth modulation (PWM) signals, which are sent to the real-time simulator, such that the velocity and attitude motion are calculated and transmitted to Pixhawk and monitoring computer, while presenting the flight scene in X-PLANE11 and plotting the velocity and attitude tracking curves on MATLAB.

In this part, three networked six-DOF fixed-wing UAVs are considered. The communication topology is illustrated in Fig. 3. The initial states are selected as $\boldsymbol{p}_1 = [20, 0, 150]^{\mathrm{T}}\mathrm{m}$, $\boldsymbol{p}_2 = [0, 20, 150]^{\mathrm{T}}\mathrm{m}$, $\boldsymbol{p}_3 = [0, -20, 150]^{\mathrm{T}}\mathrm{m}$, $V_1 = V_2 = 40\mathrm{m/s}$, $V_3 = 39.5\mathrm{m/s}$, $\boldsymbol{\varphi}_1 = [1, 0, 0]^{\mathrm{T}}\,\mathrm{deg}$, $\boldsymbol{\varphi}_2 = \boldsymbol{\varphi}_3 = [0, 0, 0]^{\mathrm{T}}\,\mathrm{deg}$, and $\boldsymbol{\omega}_1 = \boldsymbol{\omega}_2 = \boldsymbol{\omega}_3 = [0, 0, 0]^{\mathrm{T}}\,\mathrm{deg/s}$. The control objective for experimental test is twofold.

1) *Task of low altitude penetration:* Velocity tracks the trajectory $V_r = 60\mathrm{m/s}$, and the desired attitude trajectory is denoted as

$$[\phi_r, \theta_r, \psi_r]^{\mathrm{T}} = \begin{cases} [0, 0, 0]^{\mathrm{T}}\,\mathrm{deg}, & 0\mathrm{s} \le t \le 5\mathrm{s} \\ [0, -10, 0]^{\mathrm{T}}\,\mathrm{deg}, & 5\mathrm{s} < t \le 12\mathrm{s} \\ [0, 0, 0]^{\mathrm{T}}\,\mathrm{deg}, & 12\mathrm{s} < t \le 18\mathrm{s}. \end{cases}$$

The external disturbances in the velocity channel are supposed as $\boldsymbol{d}_{v3} = [0.5\sin(3t), 0.3\cos(2t), 0.6\sin(2t)]^{\mathrm{T}}$ during $t \in (6, 15]\mathrm{s}$.

2) *The following full-state constraints are achieved:* $0\mathrm{m/s} < V_i < 100\mathrm{m/s}$, $-60^\circ < \phi_i < 60^\circ$, $-60^\circ < \theta_i < 60^\circ$, $-180^\circ < \psi_i < 180^\circ$, $-10\,\mathrm{deg/s} < p_i < 10\,\mathrm{deg/s}$, $-10\,\mathrm{deg/s} < q_i < 10\,\mathrm{deg/s}$, and $-5\,\mathrm{deg/s} < r_i < 5\,\mathrm{deg/s}$.

The control law and adaptation law are provided with design parameters as $p_v = 1.4$, $p_\varphi = 1.2$, $q_v = q_\varphi = 0.8$, $c_{vi1} = c_{vi2} = 300$, $\varepsilon_{vi} = \varepsilon_{\omega i} = 0.01$, $h_{v32} = 0.001$, $\kappa_{\omega i1} = \kappa_{\omega i2} = \kappa_{\omega i3} = 0.01$, $\gamma_{v22} = \sigma_{v22} = 20$, $\boldsymbol{K}_{2i} = \boldsymbol{K}_{3i} = \mathrm{diag}\{3 \times 10^{-4}, 4 \times 10^{-4}, 5 \times 10^{-4}\}$, $\boldsymbol{K}_{4i} = \boldsymbol{K}_{5i} = \mathrm{diag}\{50, 50, 50\}$ $(t \in (0, 5], (7, 12], (14, 18])$, and $\boldsymbol{K}_{4i} = \boldsymbol{K}_{5i} = \mathrm{diag}\{2, 2, 2\}(t \in (5, 7], (12, 14])$.

Experimental results are exhibited in Fig. 4(a)–(d). Apparently, the proposed method can produce a rapid and accurate velocity and attitude tracking behavior because of the contribution of disturbance rejection and fixed-time property. In view of Fig. 4(e)–(h), the tracking errors of velocity and attitude remain in a small neighborhood of zero within fixed time. During the operation, the states strictly keep within corresponding constraints.

To highlight the superiority of the suggested control scheme, the related traditional controller in [31], FTC in [26], and finite-time FTC in [13] are taken as comparative objects under the same conditions. Taking the follower 1, for example, the actuator faults are introduced as $\boldsymbol{\rho}_{\delta 2} = \mathrm{diag}\{1,\ 0.9,\ 1\}$ during $t \in (15, 18]$. Task of coordinated turn and climb is considered: the velocity is supposed to be kept as $40\,\mathrm{m/s}$, and the attitude tracks the trajectory

$$[\phi_r, \theta_r, \psi_r]^{\mathrm{T}} = \begin{cases} [0, 0, 0]^{\mathrm{T}}\,\mathrm{deg}, & 0\,\mathrm{s} \le t \le 5\,\mathrm{s} \\ [10, 10, 10]^{\mathrm{T}}\,\mathrm{deg}, & 5\,\mathrm{s} < t \le 15\,\mathrm{s} \\ [0, 0, 10]^{\mathrm{T}}\,\mathrm{deg}, & 15\,\mathrm{s} < t \le 24\,\mathrm{s}. \end{cases}$$

Comparative simulation results are shown in Fig. 5(a)–(c). One can evidently find that although both FTC and finite-time FTC can accurately track the desired attitude commands regardless of actuator faults and disturbances, a slight rapid dynamic response and decreased tracking deviation can be discerned by the proposed scheme. What is more, it is distinct to see that no matter in transient and static phase, in contrast to severe fluctuations appearing in the traditional controller [31] and larger overshoots resulting in FTC [26], controlling oscillations are effectively accommodated with the help of FTC and fixed-time property, naturally yielding the faster convergence performance and better robustness to the actuator faults and disturbances.

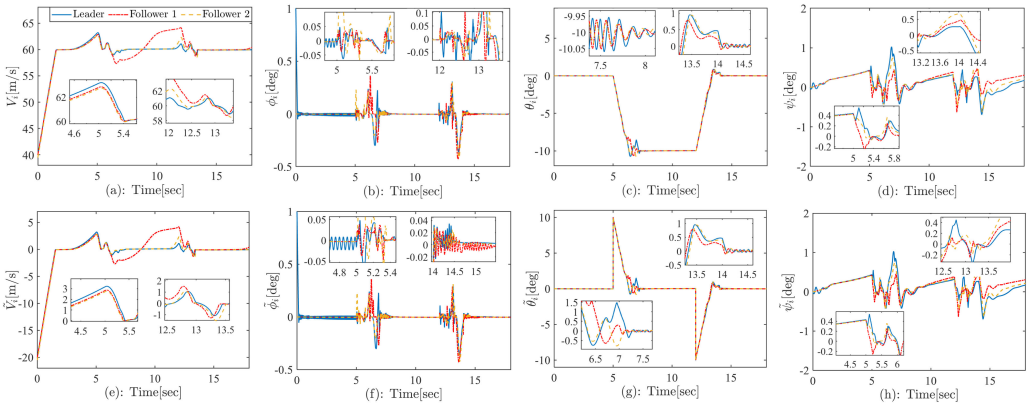

Fig. 4. Velocity and attitude tracking performance under proposed controller for experimental test. (a) V_i response. (b) ϕ_i response. (c) θ_i response. (d) ψ_i response. (e) Tracking error of V_i. (f) Tracking error of ϕ_i. (g) Tracking error of θ_i. (h) Tracking error of ψ_i.

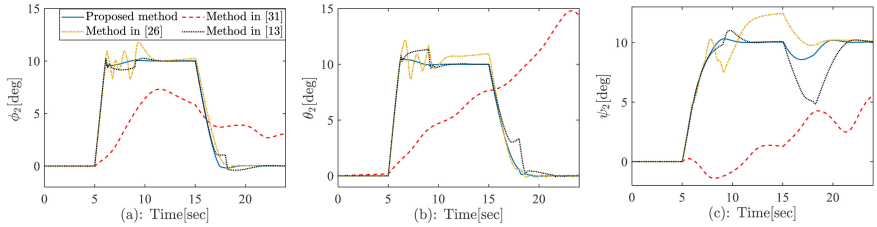

Fig. 5. Attitude tracking performances for comparison under the proposed method and methods in [13], [26], and [31]. (a) ϕ_2 response. (b) θ_2 response. (c) ψ_2 response.

V. Conclusion

An adaptive fixed-time FTC methodology has been designed for multiple six-DOF UAVs with actuator faults and constraint guarantees. Specifically, system transformation with scaling function is introduced to guarantee the states within involved constraints. The fixed-time convergence is ensured based on the transformed unconstrained system. The actuator faults as well as the network induced errors are dealt with by the bound estimation approach and some well-defined smooth functions. All closed-loop signals are SGUUB, and meanwhile, the velocity and attitude tracking are achieved by fixed time. This work lays down the groundwork for other coordinated control problems of UAVs including motion re-coordination and trajectory planning. This extension of coordinated control to guidance system for UAVs deserves further investigation. In practical flight, the communication among UAVs may be switching and directed. Future works can focus on the distributed fixed-time fault-tolerant control for multi-UAVs within a switching and directed communication. Despite that the proposed strategy is capable of tolerating actuator faults, the issues of actuator saturation and sensor fault diagnosis are not yet considered. Investigation of the aforementioned factors is our future work.

Appendix A
Proof of Theorem 1

Combined with (13), (24) further becomes

$$\dot{\xi}_{vi} = \eta_{vi}\left[\zeta_{vi}\rho_{T_i}T_{xi0} + \zeta_{vi}T_{xif} + \frac{\boldsymbol{v}_i^{\mathrm{T}}}{V_i}\left(\boldsymbol{R}_1^{\mathrm{T}}\boldsymbol{g} + \frac{\boldsymbol{F}_{i0}}{m_i}\right)\right] + \eta_{vi}\left[\frac{\boldsymbol{v}_i^{\mathrm{T}}\left(\boldsymbol{\Delta}_{vi} + \boldsymbol{d}_{vi}\right)}{V_i} - \dot{V}_r\right] + \mu_{vi} \tag{37}$$

where $\zeta_{vi} = \frac{u_i}{m_i V_i}$ and $\boldsymbol{\Delta}_{vi} = \frac{\Delta \boldsymbol{F}_i}{m_i}$.

Using Young's inequality, we obtain from (19) that

$$\frac{\xi_{vi}\eta_{vi}}{V_i}\boldsymbol{v}_i^{\mathrm{T}}\left(\boldsymbol{\Delta}_{vi} + \boldsymbol{d}_{vi}\right) \le \sum_{l=1}^{3}\left(\frac{\xi_{vi}^2\eta_{vi}^2 v_{il}^2\Phi_{vi}\boldsymbol{\varsigma}_{vil}^{\mathrm{T}}\boldsymbol{\varsigma}_{vil}}{2h_{vi1}^2V_i^2} + \frac{\xi_{vi}^2\eta_{vi}^2v_{il}^2}{2h_{vi2}^2V_i^2} + \frac{h_{vi1}^2}{2} + \frac{h_{vi2}^2\bar{\tau}_{vil}^2}{2}\right) \tag{38}$$

where $\Phi_{vi} = \max\{\boldsymbol{W}_{vi1}^{*\mathrm{T}}\boldsymbol{W}_{vi1}^{*}, \boldsymbol{W}_{vi2}^{*\mathrm{T}}\boldsymbol{W}_{vi2}^{*}, \boldsymbol{W}_{vi3}^{*\mathrm{T}}\boldsymbol{W}_{vi3}^{*}\}$ and $\tau_{vil} + d_{vil}$ satisfies $|\tau_{vil} + d_{vil}| \le \bar{\tau}_{vil}$.

From (37) and (38), taking the time derivative of $\frac{1}{2}\xi_{vi}^2$ derives

$$\xi_{vi}\dot{\xi}_{vi} \le \xi_{vi}\eta_{vi}\left[\frac{\boldsymbol{v}_i^{\mathrm{T}}}{V_i}\left(\boldsymbol{R}_1^{\mathrm{T}}\boldsymbol{g} + \frac{\boldsymbol{F}_{i0}}{m_i}\right) + \frac{\Phi_{vi}\boldsymbol{v}_i^{\mathrm{T}}\boldsymbol{\Xi}_{vi}}{2h_{vi1}^2V_i^2} + \frac{\xi_{vi}\eta_{vi}\boldsymbol{v}_i^{\mathrm{T}}\boldsymbol{v}_i}{2h_{vi2}^2V_i^2}\right] + \xi_{vi}\eta_{vi}\left(\zeta_{vi}\rho_{T_i}T_{xi0} + \zeta_{vi}T_{xif} - \dot{V}_{ri} + \frac{\mu_{vi}}{\eta_{vi}}\right) + \sum_{l=1}^{3}\left(\frac{h_{vi1}^2}{2} + \frac{h_{vi2}^2\bar{\tau}_{vil}^2}{2}\right). \tag{39}$$

Let $\beta_{vi} = 1/\rho_{T_i}$ and $g_{vi} = \beta_{vi}\sup_{t\ge 0}T_{xif}$. And define $\tilde{\Phi}_{vi} = \hat{\Phi}_{vi} - \Phi_{vi}$, $\tilde{\beta}_{vi} = \hat{\beta}_{vi} - \beta_{vi}$, and $\tilde{g}_{vi} = \hat{g}_{vi} - g_{vi}$, where $\hat{\Phi}_{vi}$, $\hat{\beta}_{vi}$, and $\hat{g}_{vi}$ are the estimations of Φ_{vi}, β_{vi}, and g_{vi}, respectively. Then, it follows that

$$\xi_{vi}\eta_{vi}\zeta_{vi}T_{xif} \le \rho_{T_i}\hat{g}_{vi}\left|\xi_{vi}\eta_{vi}\right|\zeta_{vi} - \rho_{T_i}\tilde{g}_{vi}\left|\xi_{vi}\eta_{vi}\right|\zeta_{vi}. \tag{40}$$

According to Lemma 3, $\rho_{T_i}\hat{g}_{vi}|\xi_{vi}\eta_{vi}|\zeta_{vi}$ satisfies

$$\rho_{T_i}\hat{g}_{vi}\left|\xi_{vi}\eta_{vi}\right|\zeta_{vi} \leq \rho_{T_i}\xi_{vi}\eta_{vi}\hat{g}_{vi}\zeta_{vi}\tanh\left(\frac{\xi_{vi}\eta_{vi}\hat{g}_{vi}\zeta_{vi}}{\varepsilon_{vi}}\right) + 0.2785\rho_{T_i}\varepsilon_{vi}. \tag{41}$$

Take the following Lyapunov function candidate:

$$L_1 = \frac{1}{2}\xi_{vi}^2 + \frac{1}{2\gamma_{vi1}}\tilde{\Phi}_{vi}^2 + \frac{\rho_{T_i}}{2\gamma_{vi2}}\tilde{g}_{vi}^2 + \frac{\rho_{T_i}}{2\gamma_{vi3}}\tilde{\beta}_{vi}^2. \tag{42}$$

Taking the time derivative of (42) along (39)–(41) gives

$$\begin{aligned}\dot{L}_1 = {} & \xi_{vi}\eta_{vi}\left[-\frac{c_{vi1}}{\eta_{vi}}\mathrm{sig}(\xi_{vi})^{2p_v-1} - \frac{c_{vi2}}{\eta_{vi}}\mathrm{sig}(\xi_{vi})^{2q_v-1} + \alpha_{vi}\right] \\ & + \xi_{vi}\eta_{vi}\left[\rho_{T_i}\hat{g}_{vi}\zeta_{vi}\tanh\left(\frac{\xi_{vi}\eta_{vi}\hat{g}_{vi}\zeta_{vi}}{\varepsilon_{vi}}\right) + \zeta_{vi}\rho_{T_i}T_{xi0}\right] \\ & + \frac{1}{\gamma_{vi1}}\tilde{\Phi}_{vi}\left(\dot{\hat{\Phi}}_{vi} - \frac{\gamma_{vi1}\xi_{vi}\eta_{vi}\boldsymbol{v}_i^{\mathrm{T}}\boldsymbol{\Xi}_{vi}}{2h_{vi1}^2V_i}\right) + \frac{\rho_{T_i}}{\gamma_{vi3}}\tilde{\beta}_{vi}\dot{\hat{\beta}}_{vi} \\ & + \frac{\rho_{T_i}}{\gamma_{vi2}}\tilde{g}_{vi}\left(\dot{\hat{g}}_{vi} - \gamma_{vi2}\left|\xi_{vi}\eta_{vi}\right|\zeta_{vi}\right) + 0.2785\rho_{T_i}\varepsilon_{vi} \\ & + \sum_{l=1}^{3}\left(\frac{h_{vi1}^2}{2} + \frac{h_{vi2}^2\bar{\tau}_{vil}^2}{2}\right).\end{aligned} \tag{43}$$

Invoking Lemma 3, it follows along (30) that

$$\xi_{vi}\eta_{vi}\zeta_{vi}\rho_{T_i}T_{xi0} \leq -\xi_{vi}\eta_{vii}\zeta_{vi}\rho_{T_i}\hat{g}_{vi}\tanh\left(\frac{\xi_{vi}\eta_{vi}\hat{g}_{vi}\zeta_{vi}}{\varepsilon_{vi}}\right) - \rho_{T_i}\xi_{vi}\eta_{vi}\alpha_{vi}\hat{\beta}_{vi} + 0.2785\rho_{T_i}\varepsilon_{vi}. \tag{44}$$

Noting that $-\rho_{T_i}\xi_{vi}\eta_{vi}\alpha_{vi}\hat{\beta}_{vi} = -\rho_{T_i}\xi_{vi}\eta_{vi}\alpha_{vi}\tilde{\beta}_{vi} - \xi_{vi}\eta_{vi}\alpha_{vi}$ and substituting (31)–(33) and (44) into (43) gives

$$\begin{aligned}\dot{L}_1 \leq {} & -c_{vi1}|\xi_{vi}|^{2p_v} - c_{vi2}|\xi_{vi}|^{2q_v} - \sigma_{vi1}\tilde{\Phi}_{vi}\hat{\Phi}_{vi} \\ & - \rho_{T_i}\sigma_{vi2}\tilde{g}_{vi}\hat{g}_{vi} - \rho_{T_i}\sigma_{vi3}\tilde{\beta}_{vi}\hat{\beta}_{vi} + 0.557\varepsilon_{vi}\rho_{T_i} \\ & + \sum_{l=1}^{3}\left(\frac{h_{vi1}^2}{2} + \frac{h_{vi2}^2\bar{\tau}_{vil}^2}{2}\right).\end{aligned} \tag{45}$$

Choose $\gamma_{vi1} = \frac{2\vartheta_{vi1}}{2\vartheta_{vi1}-1}$, $\gamma_{vi2} = \frac{2\vartheta_{vi2}}{2\vartheta_{vi2}-1}$, and $\gamma_{vi3} = \frac{2\vartheta_{vi3}}{2\vartheta_{vi3}-1}$ with $\vartheta_{vi1} > \frac{1}{2}$, $\vartheta_{vi2} > \frac{1}{2}$, and $\vartheta_{vi3} > \frac{1}{2}$. It holds that

$$\begin{aligned}-\sigma_{vi1}\tilde{\Phi}_{vi}\hat{\Phi}_{vi} &\leq -\frac{\sigma_{vi1}}{\gamma_{vi1}}\tilde{\Phi}_{vi}^2 + \frac{\vartheta_{vi1}\sigma_{vi1}}{2}\Phi_{vi}^2 \\ -\rho_{T_i}\sigma_{vi2}\tilde{g}_{vi}\hat{g}_{vi} &\leq -\frac{\rho_{T_i}\sigma_{vi2}}{\gamma_{vi2}}\tilde{g}_{vi}^2 + \frac{\vartheta_{vi2}\rho_{T_i}\sigma_{vi2}}{2}g_{vi}^2 \\ -\rho_{T_i}\sigma_{vi3}\tilde{\beta}_{vi}\hat{\beta}_{vi} &\leq -\frac{\rho_{T_i}\sigma_{vi3}}{\gamma_{vi3}}\tilde{\beta}_{vi}^2 + \frac{\vartheta_{vi3}\rho_{T_i}\sigma_{vi3}}{2}\beta_{vi}^2.\end{aligned} \tag{46}$$

By adding and subtracting the terms of $(\frac{\tilde{\Phi}_{vi}^2}{2\gamma_{vi1}})^{p_v}$, $(\frac{\tilde{\Phi}_{vi}^2}{2\gamma_{vi1}})^{q_v}$, $(\frac{\rho_{T_i}\tilde{g}_{vi}^2}{2\gamma_{vi2}})^{p_v}$, $(\frac{\rho_{T_i}\tilde{g}_{vi}^2}{2\gamma_{vi2}})^{q_v}$, $(\frac{\rho_{T_i}\tilde{\beta}_{vi}^2}{2\gamma_{vi3}})^{p_v}$, $(\frac{\rho_{T_i}\tilde{\beta}_{vi}^2}{2\gamma_{vi3}})^{q_v}$, and substituting (46) into (45), it follows that

$$\begin{aligned}\dot{L}_1 \leq {} & -c_{vi1}|\xi_{vi}|^{2p_v} - c_{vi2}|\xi_{vi}|^{2q_v} - \sigma_{vi1}\left(\frac{\tilde{\Phi}_{vi}^2}{2\gamma_{vi1}}\right)^{p_v} \\ & - \sigma_{vi1}\left(\frac{\tilde{\Phi}_{vi}^2}{2\gamma_{vi1}}\right)^{q_v} - \sigma_{vi2}\left(\frac{\rho_{T_i}\tilde{g}_{vi}^2}{2\gamma_{vi2}}\right)^{p_v} - \sigma_{vi2}\left(\frac{\rho_{T_i}\tilde{g}_{vi}^2}{2\gamma_{vi2}}\right)^{q_v} \\ & - \sigma_{vi3}\left(\frac{\rho_{T_i}\tilde{\beta}_{vi}^2}{2\gamma_{vi3}}\right)^{p_v} - \sigma_{vi3}\left(\frac{\rho_{T_i}\tilde{\beta}_{vi}^2}{2\gamma_{vi3}}\right)^{q_v} + \sigma_{vi1}\left(\frac{\tilde{\Phi}_{vi}^2}{2\gamma_{vi1}}\right)^{p_v} \\ & + \sigma_{vi2}\left(\frac{\rho_{T_i}\tilde{g}_{vi}^2}{2\gamma_{vi2}}\right)^{p_v} + \sigma_{vi3}\left(\frac{\rho_{T_i}\tilde{\beta}_{vi}^2}{2\gamma_{vi3}}\right)^{p_v} - \frac{\sigma_{vi1}}{2\gamma_{vi1}}\tilde{\Phi}_{vi}^2 \\ & - \frac{\rho_{T_i}\sigma_{vi2}}{2\gamma_{vi2}}\tilde{g}_{vi}^2 - \frac{\rho_{T_i}\sigma_{vi3}}{2\gamma_{vi3}}\tilde{\beta}_{vi}^2 + \frac{\vartheta_{vi1}\sigma_{vi1}}{2}\Phi_{vi}^2 \\ & + \frac{\vartheta_{vi2}\rho_{T_i}\sigma_{vi2}}{2}g_{vi}^2 + \frac{\vartheta_{vi3}\rho_{T_i}\sigma_{vi3}}{2}\beta_{vi}^2 + 0.557\varepsilon_{vi}\rho_{T_i} \\ & + \sum_{l=1}^{3}\left(\frac{h_{vi1}^2}{2} + \frac{h_{vi2}^2\bar{\tau}_{vil}^2}{2} + \sigma_{vil}\left(1-q_v\right)q_v^{\frac{q_v}{1-q_v}}\right)\end{aligned} \tag{47}$$

where the following inequalities are used from Lemma 4:

$$\begin{aligned}\left(\frac{\tilde{\Phi}_{vi}^2}{2\gamma_{vi1}}\right)^{q_v} &\leq \frac{\tilde{\Phi}_{vi}^2}{2\gamma_{vi1}} + \left(1-q_v\right)q_v^{\frac{q_v}{1-q_v}} \\ \left(\frac{\rho_{T_i}\tilde{g}_{vi}^2}{2\gamma_{vi2}}\right)^{q_v} &\leq \frac{\rho_{T_i}\tilde{g}_{vi}^2}{2\gamma_{vi2}} + \left(1-q_v\right)q_v^{\frac{q_v}{1-q_v}} \\ \left(\frac{\rho_{T_i}\tilde{\beta}_{vi}^2}{2\gamma_{vi3}}\right)^{q_v} &\leq \frac{\rho_{T_i}\tilde{\beta}_{vi}^2}{2\gamma_{vi3}} + \left(1-q_v\right)q_v^{\frac{q_v}{1-q_v}}.\end{aligned} \tag{48}$$

Suppose that there exist unknown constants Δ_{vi1}, Δ_{vi2}, and Δ_{vi3} such that $|\tilde{\Phi}_{vi}| \leq \Delta_{vi1}$, $\sqrt{\rho_{T_i}}|\tilde{g}_{vi}| \leq \Delta_{vi2}$, $\sqrt{\rho_{T_i}}|\tilde{\beta}_{vi}| \leq \Delta_{vi3}$. The following two cases are discussed.

Case 1: If $\Delta_{vi1} < \sqrt{2\gamma_{vi1}}$ or $\Delta_{vi2} < \sqrt{2\gamma_{vi2}}$ or $\Delta_{vi3} < \sqrt{2\gamma_{vi3}}$, then

$$\begin{aligned}\sigma_{vi1}\left(\frac{\tilde{\Phi}_{vi}^2}{2\gamma_{vi1}}\right)^{p_v} - \frac{\sigma_{vi1}}{2\gamma_{vi1}}\tilde{\Phi}_{vi}^2 < 0 \\ \sigma_{vi2}\left(\frac{\rho_{T_i}\tilde{g}_{vi}^2}{2\gamma_{vi2}}\right)^{p_v} - \frac{\rho_{T_i}\sigma_{vi2}}{2\gamma_{vi2}}\tilde{g}_{vi}^2 < 0 \\ \sigma_{vi3}\left(\frac{\rho_{T_i}\tilde{\beta}_{vi}^2}{2\gamma_{vi3}}\right)^{p_v} - \frac{\rho_{T_i}\sigma_{vi3}}{2\gamma_{vi3}}\tilde{\beta}_{vi}^2 < 0.\end{aligned} \tag{49}$$

Case 2: If $\Delta_{vi1} \geq \sqrt{2\gamma_{vi1}}$ or $\Delta_{vi2} \geq \sqrt{2\gamma_{vi2}}$ or $\Delta_{vi3} \geq \sqrt{2\gamma_{vi3}}$, then

$$\begin{aligned}\sigma_{vi1}\left(\frac{\tilde{\Phi}_{vi}^2}{2\gamma_{vi1}}\right)^{p_v} - \frac{\sigma_{vi1}}{2\gamma_{vi1}}\tilde{\Phi}_{vi}^2 \leq \sigma_{vi1}\left(\frac{\Delta_{vi1}^2}{2\gamma_{vi1}}\right)^{p_v} - \frac{\sigma_{vi1}}{2\gamma_{vi1}}\Delta_{vi1}^2 \\ \sigma_{vi2}\left(\frac{\rho_{T_i}\tilde{g}_{vi}^2}{2\gamma_{vi2}}\right)^{p_v} - \frac{\rho_{T_i}\sigma_{vi2}}{2\gamma_{vi2}}\tilde{g}_{vi}^2 \leq \sigma_{vi2}\left(\frac{\Delta_{vi2}^2}{2\gamma_{vi2}}\right)^{p_v} - \frac{\sigma_{vi2}}{2\gamma_{vi2}}\Delta_{vi2}^2 \\ \sigma_{vi3}\left(\frac{\rho_{T_i}\tilde{\beta}_{vi}^2}{2\gamma_{vi3}}\right)^{p_v} - \frac{\rho_{T_i}\sigma_{vi3}}{2\gamma_{vi3}}\tilde{\beta}_{vi}^2 \leq \sigma_{vi3}\left(\frac{\Delta_{vi3}^2}{2\gamma_{vi3}}\right)^{p_v} - \frac{\sigma_{vi3}}{2\gamma_{vi3}}\Delta_{vi3}^2.\end{aligned} \tag{50}$$

Summarizing the *Case 1* and *Case 2*, it can be concluded that

$$\upsilon_{vi1} = \begin{cases} 0, & \text{if } \Delta_{vi1} < \sqrt{2\gamma_{vi1}} \\ \sigma_{vi1}\left(\frac{\Delta_{vi1}^2}{2\gamma_{vi1}}\right)^{p_v} - \frac{\sigma_{vi1}}{2\gamma_{vi1}}\Delta_{vi1}^2, & \text{if } \Delta_{vi1} \geq \sqrt{2\gamma_{vi1}} \end{cases}$$

$$\upsilon_{vi2} = \begin{cases} 0, & \text{if } \Delta_{vi2} < \sqrt{2\gamma_{vi2}} \\ \sigma_{vi2}\left(\frac{\Delta_{vi2}^2}{2\gamma_{vi2}}\right)^{p_v} - \frac{\sigma_{vi2}}{2\gamma_{vi2}}\Delta_{vi2}^2, & \text{if } \Delta_{vi2} \geq \sqrt{2\gamma_{vi2}} \end{cases}$$

$$\upsilon_{vi3}=\begin{cases}0, & \text{if } \Delta_{vi3}<\sqrt{2\gamma_{vi3}}\\ \sigma_{vi3}\left(\frac{\Delta_{vi3}^2}{2\gamma_{vi3}}\right)^{p_v}-\frac{\sigma_{vi3}}{2\gamma_{vi3}}\Delta_{vi3}^2, & \text{if } \Delta_{vi3}\geq\sqrt{2\gamma_{vi3}}.\end{cases}\tag{51}$$

From (47) and (51), we see that

$$\dot{L}_1\leq-\chi_{vi1}{L_1}^{p_v}-\chi_{vi2}{L_1}^{q_v}+\chi_{vi3}\tag{52}$$

where $\chi_{vi1}=\min\{c_{vi1}2^{p_v},\sigma_{vi1},\sigma_{vi2},\sigma_{vi3}\}$, $\chi_{vi2}=\min\{c_{vi2}2^{q_v},\sigma_{vi1},\sigma_{vi2},\sigma_{vi3}\}$, and $\chi_{vi3}=\upsilon_{vi1}+\upsilon_{vi2}+\upsilon_{vi3}+\frac{\vartheta_{vi1}\sigma_{vi1}}{2}\Phi_{vi}^2+\frac{\vartheta_{vi2}\rho_{T_i}\sigma_{vi2}}{2}g_{vi}^2+\frac{\vartheta_{vi3}\rho_{T_i}\sigma_{vi3}}{2}\beta_{vi}^2+0.557\rho_{T_i}\varepsilon_{vi}+\sum_{l=1}^{3}(\frac{h_{vi1}^2}{2}+\frac{h_{vi2}^2\bar{\tau}_{vil}^2}{2}+\sigma_{vil}(1-q_v)q_v^{\frac{q_v}{1-q_v}})$.

In accordance with Lemma 1, all signals of the translational subsystem are semiglobally practically fixed-time bounded and converge to the following compact set $L_1\leq\min\{(\frac{\chi_{vi3}}{\chi_{vi1}(1-\sigma)})^{\frac{1}{p_v}},(\frac{\chi_{vi3}}{\chi_{vi2}(1-\sigma)})^{\frac{1}{q_v}}\}$, and the setting time is $T\leq T_{\max,v}:=\frac{1}{\chi_{vi1}\sigma(p_v-1)}+\frac{1}{\chi_{vi2}\sigma(1-q_v)}$. It should be noticed that $|\tilde{V}_i|$ can be made arbitrarily small by increasing c_{vi1}, c_{vi2}, γ_{vi1}, γ_{vi2}, and γ_{vi3}, and meanwhile decreasing h_{vi1}, h_{vi2}, σ_{vi1}, σ_{vi2}, σ_{vi3}, and ε_{vi}. Proper choice of p_v and q_v helps to reduce convergence time and improve convergence accuracy. This will be shown in the following numerical example. This completes the proof of Theorem 1. ■

APPENDIX B
PROOF OF THEOREM 2

The following proof comprises of the following two steps.

Step 1: Using (14), (25) and (27) yields

$$\dot{\boldsymbol{\xi}}_{\varphi i}=\boldsymbol{\eta}_{\varphi i}\left[\lambda_i\left(\boldsymbol{R}_2^{-1}\boldsymbol{K}_{1i}\boldsymbol{\xi}_{\omega i}-\dot{\boldsymbol{\varphi}}_r\right)-\lambda_{i2}\sum_{j\in\mathcal{N}_i}a_{ij}\dot{\tilde{\boldsymbol{\varphi}}}_j\right]+\boldsymbol{\mu}_{\varphi i}\tag{53}$$

where $\boldsymbol{K}_{1i}=\mathrm{diag}\{(F_{\omega i11}+\omega_{i1})(F_{\omega i12}-\omega_{i1}),(F_{\omega i21}+\omega_{i2})(F_{\omega i22}-\omega_{i2}),(F_{\omega i31}+\omega_{i3})(F_{\omega i32}-\omega_{i3})\}$.

Based on (53), we design the virtual controller $\boldsymbol{\xi}_{\omega ci}$ as

$$\begin{aligned}\boldsymbol{\xi}_{\omega ci}=&-\frac{\boldsymbol{K}_{1i}^{-1}\boldsymbol{R}_2\boldsymbol{\eta}_{\varphi i}^{-1}}{\lambda_i}\left(\boldsymbol{K}_{2i}\boldsymbol{\xi}_{\varphi i}\|\boldsymbol{\xi}_{\varphi i}\|^{2p_\varphi-2}+\boldsymbol{K}_{3i}\boldsymbol{\xi}_{\varphi i}\|\boldsymbol{\xi}_{\varphi i}\|^{2q_\varphi-2}\right)\\&-\frac{\boldsymbol{K}_{1i}^{-1}\boldsymbol{R}_2}{\lambda_i}\left(\boldsymbol{\eta}_{\varphi i}^{-1}\boldsymbol{\mu}_{\varphi i}-\lambda_i\dot{\boldsymbol{\varphi}}_r-\lambda_{i2}\sum_{j\in\mathcal{N}_i}a_{ij}\dot{\tilde{\boldsymbol{\varphi}}}_j\right).\end{aligned}\tag{54}$$

To avoid the direct differentiation of the complex $\boldsymbol{\xi}_{\omega ci}$, we introduce a new variable $\boldsymbol{\xi}_{\omega di}$ using dynamic surface control [36]. The following nonlinear filter is exploited to guarantee the overall fixed-time convergence.

$$\dot{\boldsymbol{\xi}}_{\omega di}=-\boldsymbol{\kappa}_{\omega i}\left(\boldsymbol{y}_{\omega i}\|\boldsymbol{y}_{\omega i}\|^{r_{\varphi 1}-1}+\boldsymbol{y}_{\omega i}\|\boldsymbol{y}_{\omega i}\|^{r_{\varphi 2}-1}\right).\tag{55}$$

Let $\boldsymbol{e}_{\omega i}=\boldsymbol{\xi}_{\omega i}-\boldsymbol{\xi}_{\omega di}$. Substituting (54) and (55) into (53), the time derivative of $\frac{1}{2}\boldsymbol{\xi}_{\varphi i}^{\mathrm{T}}\boldsymbol{\xi}_{\varphi i}$ denotes

$$\begin{aligned}\boldsymbol{\xi}_{\varphi i}^{\mathrm{T}}\dot{\boldsymbol{\xi}}_{\varphi i}=&-\boldsymbol{\xi}_{\varphi i}^{\mathrm{T}}\left(\boldsymbol{K}_{2i}\boldsymbol{\xi}_{\varphi i}\|\boldsymbol{\xi}_{\varphi i}\|^{2p_\varphi-2}+\boldsymbol{K}_{3i}\boldsymbol{\xi}_{\varphi i}\|\boldsymbol{\xi}_{\varphi i}\|^{2q_\varphi-2}\right)\\&+\lambda_i\boldsymbol{\xi}_{\varphi i}^{\mathrm{T}}\boldsymbol{\eta}_{\varphi i}\boldsymbol{R}_2^{-1}\boldsymbol{K}_{1i}\left(\boldsymbol{e}_{\omega i}+\boldsymbol{y}_{\omega i}\right).\end{aligned}\tag{56}$$

Step 2: Differentiating $\frac{1}{2}\boldsymbol{e}_{\omega i}^{\mathrm{T}}\boldsymbol{e}_{\omega i}$ along (18) and (29) gives

$$\begin{aligned}\boldsymbol{e}_{\omega i}^{\mathrm{T}}\dot{\boldsymbol{e}}_{\omega i}=&\ \boldsymbol{e}_{\omega i}^{\mathrm{T}}\boldsymbol{\eta}_{\omega i}\boldsymbol{J}_{i0}^{-1}\boldsymbol{C}_0\boldsymbol{\rho}_{\delta_i}\boldsymbol{\delta}_{i0}+\boldsymbol{J}_{i0}^{-1}\boldsymbol{S}\left(\boldsymbol{J}_{i0}\boldsymbol{\omega}_i\right)+\boldsymbol{J}_{i0}^{-1}\boldsymbol{N}_{i0}\\&+\boldsymbol{e}_{\omega i}^{\mathrm{T}}\left[\boldsymbol{\eta}_{\omega i}\left(\boldsymbol{\Delta}_{\omega i}'+\boldsymbol{l}_{\omega i}+\boldsymbol{d}_{\omega i}\right)+\boldsymbol{\mu}_{\omega i}-\dot{\boldsymbol{\xi}}_{\omega di}\right].\end{aligned}\tag{57}$$

Using Young's inequality, it holds along (19) that

$$\begin{aligned}\boldsymbol{e}_{\omega i}^{\mathrm{T}}\boldsymbol{\eta}_{\omega i}\left(\boldsymbol{\Delta}_{\omega i}'+\boldsymbol{l}_{\omega i}+\boldsymbol{d}_{\omega i}\right)\leq&\ \boldsymbol{e}_{\omega i}^{\mathrm{T}}\boldsymbol{\eta}_{\omega i}\left(\frac{\Phi_{\omega i}\boldsymbol{\Xi}_{\omega i}}{2h_{\omega i1}^2}+\frac{\boldsymbol{\eta}_{\omega i}^{\mathrm{T}}\boldsymbol{e}_{\omega i}}{2h_{\omega i2}^2}\right)\\&+\sum_{l=1}^{3}\left(\frac{h_{\omega i1}^2}{2}+\frac{h_{\omega i2}^2\bar{\tau}_{\omega il}^2}{2}\right)\end{aligned}\tag{58}$$

where $\Phi_{\omega i}=\max\{\boldsymbol{W}_{\omega i1}^{*\mathrm{T}}\boldsymbol{W}_{\omega i1}^{*},\boldsymbol{W}_{\omega i2}^{*\mathrm{T}}\boldsymbol{W}_{\omega i2}^{*},\boldsymbol{W}_{\omega i3}^{*\mathrm{T}}\boldsymbol{W}_{\omega i3}^{*}\}$ and there exists $|\tau_{\omega il}+l_{\omega il}+d_{\omega il}|\leq\bar{\tau}_{\omega il}$.

According to the Assumption 2, we define $g_{\omega i}=\inf_{t\geq0}\lambda_{\min}(\boldsymbol{J}_{i0}^{-1}\boldsymbol{C}_0(\boldsymbol{\delta}_i)\boldsymbol{\rho}_{\delta_i}(\boldsymbol{J}_{i0}^{-1}\boldsymbol{C}_0(\boldsymbol{\delta}_i))^{\mathrm{T}})$ and $\beta_{\omega i}=1/g_{\omega i}$. Let $\tilde{\Phi}_{\omega i}=\hat{\Phi}_{\omega i}-\Phi_{\omega i}$ and $\tilde{\beta}_{\omega i}=\hat{\beta}_{\omega i}-\beta_{\omega i}$ with $\hat{\Phi}_{\omega i}$ and $\hat{\beta}_{\omega i}$ being the estimations of $\Phi_{\omega i}$ and $\beta_{\omega i}$, respectively.

Consider the Lyapunov function candidate as

$$L_2=\frac{1}{2}\boldsymbol{\xi}_{\varphi i}^{\mathrm{T}}\boldsymbol{\xi}_{\varphi i}+\frac{1}{2}\boldsymbol{e}_{\omega i}^{\mathrm{T}}\boldsymbol{e}_{\omega i}+\frac{1}{2}\boldsymbol{y}_{\omega i}^{\mathrm{T}}\boldsymbol{y}_{\omega i}+\frac{1}{2\gamma_{\omega i1}}\tilde{\Phi}_{\omega i}^2+\frac{g_{\omega i}}{2\gamma_{\omega i2}}\tilde{\beta}_{\omega i}^2.\tag{59}$$

From (56)–(58), taking the time derivative of (59) gives

$$\begin{aligned}\dot{L}_2\leq&-\boldsymbol{\xi}_{\varphi i}^{\mathrm{T}}\left(\boldsymbol{K}_{2i}\boldsymbol{\xi}_{\varphi i}\|\boldsymbol{\xi}_{\varphi i}\|^{2p_\varphi-2}+\boldsymbol{K}_{3i}\boldsymbol{\xi}_{\varphi i}\|\boldsymbol{\xi}_{\varphi i}\|^{2q_\varphi-2}\right)+\boldsymbol{e}_{\omega i}^{\mathrm{T}}\boldsymbol{\zeta}_{\omega i}\\&-\boldsymbol{e}_{\omega i}^{\mathrm{T}}\left(\boldsymbol{K}_{4i}\boldsymbol{e}_{\omega i}\|\boldsymbol{e}_{\omega i}\|^{2p_\varphi-2}+\boldsymbol{K}_{5i}\boldsymbol{e}_{\omega i}\|\boldsymbol{e}_{\omega i}\|^{2q_\varphi-2}\right)\\&+\boldsymbol{e}_{\omega i}^{\mathrm{T}}\boldsymbol{\eta}_{\omega i}\boldsymbol{J}_{i0}^{-1}\boldsymbol{C}_0\boldsymbol{\rho}_{\delta_i}\boldsymbol{\delta}_{i0}-\boldsymbol{e}_{\omega i}^{\mathrm{T}}\frac{\tilde{\Phi}_{\omega i}\boldsymbol{\eta}_{\omega i}\boldsymbol{\Xi}_{\omega i}}{2h_{\omega i1}^2}\\&+\boldsymbol{y}_{\omega i}^{\mathrm{T}}\left[\dot{\boldsymbol{y}}_{\omega i}+\lambda_i\boldsymbol{K}_{1i}^{\mathrm{T}}\left(\boldsymbol{R}_2^{-1}\right)^{\mathrm{T}}\boldsymbol{\eta}_{\varphi i}^{\mathrm{T}}\boldsymbol{\xi}_{\varphi i}\right]\\&+\frac{1}{\gamma_{\omega i1}}\tilde{\Phi}_{\omega i}\dot{\hat{\Phi}}_{\omega i}+\frac{g_{\omega i}}{\gamma_{\omega i2}}\tilde{\beta}_{\omega i}\dot{\hat{\beta}}_{\omega i}\\&+\sum_{l=1}^{3}\left(\frac{h_{\omega i1}^2}{2}+\frac{h_{\omega i2}^2\bar{\tau}_{\omega il}^2}{2}\right).\end{aligned}\tag{60}$$

In (60), define $\boldsymbol{\alpha}_{\varphi i}=\lambda_i\boldsymbol{K}_{1i}^{\mathrm{T}}(\boldsymbol{R}_2^{-1})^{\mathrm{T}}\boldsymbol{\eta}_{\varphi i}^{\mathrm{T}}\boldsymbol{\xi}_{\varphi i}$. Noting that the inequality holds: $x\leq x^m+x^n$, where $x\geq0$, $0<m<1$, and $n>1$, it follows that

$$\boldsymbol{y}_{\omega i}^{\mathrm{T}}\left(\dot{\boldsymbol{y}}_{\omega i}+\boldsymbol{\alpha}_{\varphi i}\right)\leq-\kappa_{\omega i}\left(\|\boldsymbol{y}_{\omega i}\|^{r_{\varphi 1}+1}+\|\boldsymbol{y}_{\omega i}\|^{r_{\varphi 2}+1}\right)+\frac{\varpi_{\omega i}^2}{2}\tag{61}$$

where $\kappa_{\omega i}=\lambda_{\min}(\boldsymbol{\kappa}_{\omega i})-1/2$ and there exists a positive constant $\varpi_{\omega i}$ such that $\|\boldsymbol{\alpha}_{\varphi i}-\boldsymbol{\xi}_{\omega ci}\|\leq\varpi_{\omega i}$.

Using (34) and invoking Lemma 2, the term of $\boldsymbol{e}_{\omega i}^{\mathrm{T}}\boldsymbol{\eta}_{\omega i}\boldsymbol{J}_{i0}^{-1}\boldsymbol{C}_0\boldsymbol{\rho}_{\delta_i}\boldsymbol{\delta}_{i0}$ renders

$$\begin{aligned}&\boldsymbol{e}_{\omega i}^{\mathrm{T}}\boldsymbol{\eta}_{\omega i}\boldsymbol{J}_{i0}^{-1}\boldsymbol{C}_0\boldsymbol{\rho}_{\delta_i}\boldsymbol{\delta}_{i0}=-\boldsymbol{e}_{\omega i}^{\mathrm{T}}\boldsymbol{\eta}_{\omega i}\boldsymbol{J}_{i0}^{-1}\boldsymbol{C}_0\boldsymbol{\rho}_{\delta_i}\left(\boldsymbol{J}_{i0}^{-1}\boldsymbol{C}_0\right)^{\mathrm{T}}\boldsymbol{\eta}_{\omega i}^{-1}\cdot\\&\frac{\boldsymbol{e}_{\omega i}\hat{\beta}_{\omega i}^2\boldsymbol{\zeta}_{\omega i}^{\mathrm{T}}\boldsymbol{\zeta}_{\omega i}}{\sqrt{\hat{\beta}_{\omega i}^2\boldsymbol{e}_{\omega i}^{\mathrm{T}}\boldsymbol{e}_{\omega i}\boldsymbol{\zeta}_{\omega i}^{\mathrm{T}}\boldsymbol{\zeta}_{\omega i}+\varepsilon_{\omega i}}}\leq-\frac{g_{\omega i}\hat{\beta}_{\omega i}^2\boldsymbol{e}_{\omega i}^{\mathrm{T}}\boldsymbol{e}_{\omega i}\boldsymbol{\zeta}_{\omega i}^{\mathrm{T}}\boldsymbol{\zeta}_{\omega i}}{\sqrt{\hat{\beta}_{\omega i}^2\boldsymbol{e}_{\omega i}^{\mathrm{T}}\boldsymbol{e}_{\omega i}\boldsymbol{\zeta}_{\omega i}^{\mathrm{T}}\boldsymbol{\zeta}_{\omega i}+\varepsilon_{\omega i}}}\\&\leq g_{\omega i}\sqrt{\varepsilon_{\omega i}}-g_{\omega i}|\hat{\beta}_{\omega i}|\,\|\boldsymbol{e}_{\omega i}\|\,\|\boldsymbol{\zeta}_{\omega i}\|\\&\leq g_{\omega i}\sqrt{\varepsilon_{\omega i}}-g_{\omega i}\hat{\beta}_{\omega i}\boldsymbol{e}_{\omega i}^{\mathrm{T}}\boldsymbol{\zeta}_{\omega i}.\end{aligned}\tag{62}$$

Based on $g_{\omega i}(\hat{\beta}_{\omega i}-\tilde{\beta}_{\omega i})=g_{\omega i}\beta_{\omega i}=1$, substitute (35), (36), (61), and (62) into (60). With the similar operations of (46)–(48), it holds that

$$\begin{aligned}\dot{L}_2 \leq & -\lambda_{\min}\left(\boldsymbol{K}_{2i}\right)\left\|\boldsymbol{\xi}_{\varphi i}\right\|^{2p_\varphi}-\lambda_{\min}\left(\boldsymbol{K}_{3i}\right)\left\|\boldsymbol{\xi}_{\varphi i}\right\|^{2q_\varphi}\\ &-\lambda_{\min}\left(\boldsymbol{K}_{4i}\right)\left\|\boldsymbol{e}_{\omega i}\right\|^{2p_\varphi}-\lambda_{\min}\left(\boldsymbol{K}_{5i}\right)\left\|\boldsymbol{e}_{\omega i}\right\|^{2q_\varphi}\\ &-\kappa_{\omega i}\|\boldsymbol{y}_{\omega i}\|^{r_{\varphi 1}+1}-\kappa_{\omega i}\|\boldsymbol{y}_{\omega i}\|^{r_{\varphi 2}+1}+g_{\omega i}\sqrt{\varepsilon_{\omega i}}\\ &-\sigma_{\omega i1}\left(\frac{\tilde{\Phi}_{\omega i}^2}{2\gamma_{\omega i1}}\right)^{p_\varphi}-\sigma_{\omega i1}\left(\frac{\tilde{\Phi}_{\omega i}^2}{2\gamma_{\omega i1}}\right)^{q_\varphi}-\sigma_{\omega i2}\left(\frac{g_{\omega i}\tilde{\beta}_{\omega i}^2}{2\gamma_{\omega i2}}\right)^{p_\varphi}\\ &-\sigma_{\omega i2}\left(\frac{g_{\omega i}\tilde{\beta}_{\omega i}^2}{2\gamma_{\omega i2}}\right)^{q_\varphi}+\sigma_{\omega i1}\left(\frac{\tilde{\Phi}_{\omega i}^2}{2\gamma_{\omega i1}}\right)^{p}+\sigma_{\omega i2}\left(\frac{g_{\omega i}\tilde{\beta}_{\omega i}^2}{2\gamma_{\omega i2}}\right)^{p_\varphi}\\ &-\frac{\sigma_{\omega i1}}{2\gamma_{\omega i1}}\tilde{\Phi}_{\omega i}^2-\frac{g_{\omega i}\sigma_{\omega i2}}{2\gamma_{\omega i2}}\tilde{\beta}_{\omega i}^2+\frac{\vartheta_{\omega i1}\sigma_{\omega i1}}{2}\Phi_{\omega i}^2\\ &+\frac{\vartheta_{\omega i2}g_{\omega i}\sigma_{\omega i2}}{2}\beta_{\omega i}^2+\sum_{l=1}^{2}\sigma_{\omega il}\left(1-q_\varphi\right)q_\varphi^{\frac{q_\varphi}{1-q_\varphi}}\\ &+\sum_{l=1}^{3}\left(\frac{h_{\omega i1}^2}{2}+\frac{h_{\omega i2}^2\bar{\tau}_{\omega il}^2}{2}\right)+\frac{\varpi_{\omega i}^2}{2}. \end{aligned}\tag{63}$$

Suppose that there exists unknown constants $\Delta_{\omega i1},\Delta_{\omega i2}$ such that $|\tilde{\Phi}_{\omega i}|\leq\Delta_{\omega i1}$, $\sqrt{g_{\omega i}}|\tilde{\beta}_{\omega i}|\leq\Delta_{\omega i2}$. Following the *Case 1* and *Case 2* in (49) and (50), one has

$$\begin{aligned}\upsilon_{\omega i1}&=\begin{cases}0, & \text{if } \Delta_{\omega i1}<\sqrt{2\gamma_{\omega i1}}\\ \sigma_{\omega i1}\left(\frac{\Delta_{\omega i1}^2}{2\gamma_{\omega i1}}\right)^{p_\varphi}-\frac{\sigma_{\omega i1}}{2\gamma_{\omega i1}}\Delta_{\omega i1}^2, & \text{if } \Delta_{\omega i1}\geq\sqrt{2\gamma_{\omega i1}}\end{cases}\\ \upsilon_{\omega i2}&=\begin{cases}0, & \text{if } \Delta_{\omega i2}<\sqrt{2\gamma_{\omega i2}}\\ \sigma_{\omega i2}\left(\frac{\Delta_{\omega i2}^2}{2\gamma_{\omega i2}}\right)^{p_\varphi}-\frac{\sigma_{\omega i2}}{2\gamma_{\omega i2}}\Delta_{\omega i2}^2, & \text{if } \Delta_{\omega i2}\geq\sqrt{2\gamma_{\omega i2}}.\end{cases}\end{aligned}\tag{64}$$

Choosing $\frac{r_{\varphi 1}+1}{2}=q_\varphi$ and $\frac{r_{\varphi 2}+1}{2}=p_\varphi$ and substituting (64) into (63), it can be checked that

$$\dot{L}_2\leq-\chi_{\omega i1}L_2^{p_\varphi}-\chi_{\omega i2}L_2^{q_\varphi}+\chi_{\omega i3}\tag{65}$$

where $\chi_{\omega i1}=\min\{\lambda_{\min}(\boldsymbol{K}_{2i})2^{p_\varphi},\ \lambda_{\min}(\boldsymbol{K}_{4i})2^{p_\varphi},\ \kappa_{\omega i}2^{p_\varphi},\ \sigma_{\omega i1},\ \sigma_{\omega i2}\}$, $\chi_{\omega i2}=\min\{\lambda_{\min}(\boldsymbol{K}_{3i})2^{q_\varphi},\ \lambda_{\min}(\boldsymbol{K}_{5i})2^{q_\varphi},\ \kappa_{\omega i}2^{q_\varphi},\sigma_{\omega i1},\sigma_{\omega i2}\}$, and $\chi_{vi3}=\upsilon_{\omega i1}+\upsilon_{\omega i2}+\frac{\vartheta_{\omega i1}\sigma_{\omega i1}}{2}\Phi_{\omega i}^2+\frac{\vartheta_{\omega i2}g_{\omega i}\sigma_{\omega i2}}{2}\beta_{\omega i}^2+g_{\omega i}\sqrt{\varepsilon_{\omega i}}+\sum_{l=1}^{3}(\frac{h_{\omega i1}^2}{2}+\frac{h_{\omega i2}^2\bar{\tau}_{\omega il}^2}{2})+\frac{\varpi_{\omega i}^2}{2}+\sum_{l=1}^{2}\sigma_{\omega il}(1-q_\varphi)q_\varphi^{\frac{q_\varphi}{1-q_\varphi}}$.

Along similar lines as Lemma 1, all signals of the rotational subsystem are semiglobally practically fixed-time bounded and converge to the following compact set $L_2\leq\min\{(\frac{\chi_{\omega i3}}{\chi_{\omega i1}(1-\sigma)})^{\frac{1}{p_\varphi}},(\frac{\chi_{\omega i3}}{\chi_{\omega i2}(1-\sigma)})^{\frac{1}{q_\varphi}}\}$, and the setting time is $T\leq T_{\max,\varphi}:=\frac{1}{\chi_{\omega i1}\sigma(p_\varphi-1)}+\frac{1}{\chi_{\omega i2}\sigma(1-q_\varphi)}$. Note that the convergence region of $\boldsymbol{e}_{\varphi i}$ can be made smaller by increasing $\boldsymbol{K}_{2i}$, $\boldsymbol{K}_{3i}$, $\boldsymbol{K}_{4i}$, $\boldsymbol{K}_{5i}$, $\gamma_{\omega i1}$, and $\gamma_{\omega i2}$, and meanwhile, decreasing $h_{\omega i1}$, $h_{\omega i2}$, $\sigma_{\omega i1}$, $\sigma_{\omega i2}$, and $\varepsilon_{\omega i}$. Thus, the attitude synchronization tracking error can be made as small as desired by appropriate choice of the design parameters. Moreover, the choice of p_φ and q_φ requires to balance the control amplitude and convergence time simultaneously. This completes the proof of Theorem 2. ■

REFERENCES

[1] J. Lwowski, A. Majumdar, P. Benavidez, J. J. Prevost, and M. Jamshidi, "Bird flocking inspired formation control for unmanned aerial vehicles using stereo camera," *IEEE Syst. J.*, vol. 13, no. 3, pp. 3580–3589, Sep. 2019.

[2] J. Zhang and J. Yan, "A novel control approach for flight-stability of fixed-wing UAV formation with wind field," *IEEE Syst. J.*, vol. 15, no. 2, pp. 2098–2108, Jun. 2021.

[3] Y. Wang, M. Shan, and D. Wang, "Motion capability analysis for multiple fixed-wing UAV formations with speed and heading rate constraints," *IEEE Control Netw. Syst.*, vol. 7, no. 2, pp. 977–989, Jun. 2020.

[4] Z. Yu *et al.*, "Fractional-order adaptive fault-tolerant synchronization tracking control of networked fixed-wing UAVs against actuator-sensor faults via intelligent learning mechanism," *IEEE Trans. Neural Netw. Learn. Syst.*, to be published, doi: 10.1109/TNNLS.2021.3059933.

[5] F. Mohseni, A. Doustmohammadi, and M. B. Menhaj, "Distributed receding horizon coverage control for multiple mobile robots," *IEEE Syst. J.*, vol. 10, no. 1, pp. 198–207, Mar. 2016.

[6] M. Lv, B. De Schutter, C. Shi, and S. Baldi, "Logic-based distributed switching control for agents in power chained form with multiple unknown control directions," *Automatica*, to be published, 2021.

[7] Z. Yu, Y. Zhang, Z. Liu, Y. Qu, and C. Y. Su, "Distributed adaptive fractional-order fault tolerant cooperative control of networked unmanned aerial vehicles via fuzzy neural networks," *IET Control Theory Appl.*, vol. 13, no. 17, pp. 2917–2929, 2019.

[8] Z. Yu, Y. Qu, and Y. Zhang, "Distributed fault-tolerant cooperative control for multi-UAVs under actuator fault and input saturation," *IEEE Trans. Control Syst. Technol.*, vol. 27, no. 6, pp. 2417–2429, Nov. 2019.

[9] Y. Wang, T. Zhang, Z. Cai, J. Zhao, and K. Wu, "Multi-UAV coordination control by chaotic grey wolf optimization based distributed MPC with event-triggered strategy," *Chin. J. Aeronaut.*, vol. 33, no. 11, pp. 2877–2897, 2020.

[10] T. Z. Muslimov and R. A. Munasypov, "Adaptive decentralized flocking control of multi-UAV circular formations based on vector fields and backstepping," *ISA Trans.*, vol. 107, pp. 143–159, 2020.

[11] H. Chen, X. Wang, L. Shen, and Y. Cong, "Formation flight of fixed-wing UAV swarms: A group-based hierarchical approach," *Chin. J. Aeronaut.*, vol. 34, no. 2, pp. 504–515, 2021.

[12] T. Z. Muslimov and R. A. Munasypov, "Consensus-based cooperative control of parallel fixed-wing UAV formations via adaptive backstepping," *Aerosp. Sci. Technol.*, vol. 109, 2021, Art. no. 106416.

[13] Z. Yu, Y. Zhang, Z. Liu, Y. Qu, C. Y. Su, and B. Jiang, "Decentralized finite-time adaptive fault-tolerant synchronization tracking control for multiple UAVs with prescribed performance," *J. Franklin Inst.*, vol. 357, no. 16, pp. 11830–11862, 2020.

[14] X. Yu, J. Yang, and S. Li, "Finite-time path following control for small-scale fixed-wing UAVs under wind disturbances," *J. Franklin Inst.*, vol. 357, no. 12, pp. 7879–7903, 2020.

[15] Z. Yu, Z. Liu, Y. Zhang, Y. Qu, and C. Y. Su, "Distributed finite-time fault-tolerant containment control for multiple unmanned aerial vehicles," *IEEE Trans. Neural Netw. Learn. Syst.*, vol. 31, no. 6, pp. 2077–2091, Jun. 2020.

[16] A. Polyakov, "Nonlinear feedback design for fixed-time stabilization of linear control systems," *IEEE Trans. Automat. Control*, vol. 57, no. 8, pp. 2106–2110, Aug. 2012.

[17] A. M. Zou, K. D. Kumar, and A. H. J. Ruiter, "Fixed-time attitude tracking control for rigid spacecraft," *Automatica*, 2020. vol. 113, 2020, Art. no. 108792.

[18] J. Zhang, S. Yu, Y. Yan, and D. Wu, "Fixed-time output feedback sliding mode tracking control of marine surface vessels under actuator faults with disturbance cancellation," *Appl. Ocean Res.*, vol. 104, 2020, Art. no. 102378.

[19] N. Wang and H. Li, "Leader-follower formation control of surface vehicles: A fixed-time control approach," *ISA Trans.*, 2020. [Online]. Available: https://doi.org/10.1016/j.isatra.2020.05.042

[20] M. Van and D. Ceglarek, "Robust fault tolerant control of robot manipulators with global fixed-time convergence," *J. Franklin Inst.*, 2020. [Online]. Available: https://doi.org/10.1016/j.jfranklin.2020.11.002

[21] Z. Cai, L. Wang, J. Zhao, K. Wu, and Y. Wang, "Virtual target guidance-based distributed model predictive control for formation control of multiple UAVs," *Chin. J. Aeronaut.*, vol. 33, no. 3, pp. 1037–1056, 2020.

[22] M. Burger and M. Guay, "Robust constraint satisfaction for continuous-time nonlinear systems in strict feedback form," *IEEE Trans. Automat. Control*, vol. 55, no. 11, pp. 2597–2601, Nov. 2010.

[23] W. He, Z. Yin, and C. Sun, "Adaptive neural network control of a marine vessel with constraints using the asymmetric barrier Lyapunov function," *IEEE Trans. Cybern.*, vol. 47, no. 7, pp. 1641–1651, Jul. 2017.
[24] K. Zhao and Y. D. Song, "Removing the feasibility conditions imposed on tracking control designs for state-constrained strict-feedback systems," *IEEE Trans. Autom. Control*, vol. 64, no. 3, pp. 1265–1272, Mar. 2019.
[25] Y, Cao, Y. Song and C. Wen, "Practical tracking control of perturbed uncertain nonaffine systems with full state constraints," *Automatica*, vol. 110, 2019, Art. no. 108608.
[26] Z. Yu *et al.*, "Decentralized fractional-order backstepping fault-tolerant control of multi-UAVs against actuator faults and wind effects," *Aerosp. Sci. Technol.*, vol. 104, 2020, Art. no. 105939.
[27] S. Zeghlache, H. Mekki, A. Bougueera, and A. Djerioui, "Actuator fault tolerant control using adaptive RBFNN fuzzy sliding mode controller for coaxial octorotor UAV," *ISA Trans.*, vol. 8, pp. 267–278, 2018.
[28] Z. Yu *et al.*, "Distributed adaptive fault-tolerant close formation flight control of multiple trailing fixed-wing UAVs," *ISA Trans.*, vol. 106, pp. 181–199, 2020.
[29] Z. Yu *et al.*, "Nussbaum-based finite-time fractional-order backstepping fault-tolerant flight control of fixed-wing UAV against input saturation with hardware-in-the-loop validation," *Mech. Syst. Signal Process.*, vol. 153, 2021, Art. no. 107406.
[30] H. Yang, B. Jiang, H. Yang, and H. H. Liu, "Synchronization of multiple 3-DoF helicopters under actuator faults and saturations with prescribed performance," *ISA Trans.*, vol. 75, pp. 118–126, 2018.
[31] O. Espen, S. Rune and K. Raymond, "Underactuated waypoint tracking of a fixed-wing UAV," *IFAC Proc.*, vol. 46, no. 30, pp. 126–133, 2015.
[32] H. Castaneda, O. S. Salas-Pena, and J. Leon-Morales, "Extended observer based on adaptive second order sliding mode control for a fixed wing UAV," *ISA Trans.*, vol. 66, pp. 226–232, 2017.
[33] H. Wang, P. X. Liu, X. Zhao, and X. Liu, "Adaptive fuzzy finite-time control of nonlinear systems with actuator faults," *IEEE Trans. Cybern.*, vol. 50, no. 5, pp. 1786–1797, May 2020.
[34] X. Yu, P. Li and Y. Zhang, "The design of fixed-time observer and finite-time fault-tolerant control for hypersonic gliding vehicles," *IEEE Trans. Ind. Electron.*, vol. 65, no. 5, pp. 4135–4144, May 2018.
[35] M. Lv, W. Yu, J. Cao, and S. Baldi, "A separation-based methodology to consensus tracking of switched high-order nonlinear multi-agent systems," *IEEE Trans. Neural Netw. Learn. Syst.*, to be published, doi: 10.1109/TNNLS.2021.3070824.
[36] M. Lv, W. Yu, J. Cao, and S. Baldi, "Consensus in high-power multi-agent systems with mixed unknown control directions via hybrid Nussbaum-based control," *IEEE Trans. Cybern.*, to be published, doi: 10.1109/TCYB.2020.3028171.
[37] D. Ba, Y. X. Li, and S. Tong, "Fixed-time adaptive neural tracking control for a class of uncertain nonstrict nonlinear systems," *Neurocomputing*, vol. 363, pp. 273–280, 2019.
[38] C. Wang and Y. Lin, "Decentralized adaptive tracking control for a class of interconnected nonlinear time-varying systems," *Automatica*, vol. 54, pp. 16–24, 2015.
[39] S. S. Ge and C. Wang, "Adaptive NN control of uncertain nonlinear pure-feedback systems," *Automatica*, vol. 38, no. 4, pp. 671–682, 2002.
[40] H. Wang and Q. Zhu, "Adaptive output feedback control of stochastic nonholonomic systems with nonlinear parameterization," *Automatica*, vol. 98, pp. 247–255, 2018.

Boyang Zhang received the B.Eng. degree in electrical engineering and automation, in 2017, from the Department of Aerospace Engineering, Air Force Engineering University, Xian, China, where he is currently working toward the Ph.D. degree in control science and engineering with the Department of Equipment Management and Unmanned Vehicle Aerial Engineering.

His research interests include the model predictive control and coordinated control of unmanned aerial vehicles.

Xiuxia Sun received the Ph.D. degree in control science and engineering from Beihang University, Beijing, China, in 1999.

She is currently a Professor with the Department of Equipment Management and Unmanned Aerial Vehicle Engineering, Air Force Engineering University, Xi'an, China. Her research interests include robust control, adaptive control, cooperative guidance navigation, and control of unmanned aerial vehicles.

Maolong Lv received the B.Sc. degree in electrical engineering and automation and the M.Sc. degree in control science and engineering from Air Force Engineering University, Xi'an, China, in 2014 and 2016, respectively, and the Ph.D. degree in intelligent control from the Delft Center for Systems and Control, Delft University of Technology, Delft, The Netherlands, in 2021.

He is currently with the College of Air Traffic Control and Navigation, Air Force Engineering University. His research interests include adaptive learning control, deep reinforcement learning, and intelligent decision with applications in multiagent systems, hypersonic flight, vehicles, unmanned autonomous system, etc.

Dr. Lv was the recipient of Descartes Excellence Fellowship from the French Government in 2018, which allowed him a research visit and a cooperation with the University of Grenoble on the topic of adaptive networked systems with emphasis on ring stability analysis for mixed traffic with human driven and autonomous vehicles from 2018 to 2019.

Shuguang Liu received the Ph.D. degree in control science and engineering from Air Force Engineering University, Xi'an, China, in 2010.

He is currently a Professor with the Department of Equipment Management and Unmanned Aerial Vehicle Engineering, Air Force Engineering University.

His research interests include the autonomous flight control theory of unmanned aerial vehicles.

Le Li received the B.Sc. degree in automation and the M.Sc. degree in control theory and control engineering from Northwestern Polytechnical University (NWPU), Xi'an, China, in 2008 and 2011, respectively, and the Ph.D. degree in model predictive control for traffic networks from Delft Center for Systems and Control, Delft University of Technology, Delft, The Netherlands, in 2016.

He is currently an Assistant Professor with Control Science and Engineering, NWPU. His research interests include model predictive control and distributed optimization with applications in robots and intelligent transportation systems.